

000 001 002 003 004 005 006 007 008 009 010 011 012 013 014 015 016 017 018 019 020 021 022 023 024 025 026 027 028 029 030 031 032 033 034 035 036 037 038 039 040 041 042 043 044 045 046 047 048 049 050 051 052 053 SEPARATE: A SIMPLE LOW-RANK PROJECTION FOR GRADIENT COMPRESSION IN MODERN LARGE-SCALE MODEL TRAINING PROCESS

Anonymous authors

Paper under double-blind review

ABSTRACT

Training Large Language Models (LLMs) presents a significant communication bottleneck, predominantly due to the growing scale of the gradient to communicate across multi-device clusters. However, how to mitigate communication overhead in practice remains a formidable challenge due to the weakness of the methodology of the existing compression methods, especially the neglect of the characteristics of the gradient. In this paper, we consider and demonstrate the low-rank properties of gradient and Hessian observed in LLMs training dynamic, and take advantage of such natural properties to design SEPARATE, a simple low-rank projection for gradient compression in modern large-scale model training processes. SEPARATE realizes dimensional reduction by common random Gaussian variables and an improved moving average error-feedback technique. We theoretically demonstrate that SEPARATE-based optimizers maintain the original convergence rate for SGD and Adam-Type optimizers for general non-convex objectives. Experimental results show that SEPARATE accelerates training speed by up to 2 \times for GPT-2-Medium pre-training, and improves performance on various benchmarks for LLAMA2-7B fine-tuning.

1 INTRODUCTION

With massive amounts of data, billions of parameters, and multi-device clusters, the remarkable strides of Large Language Models (LLMs) across multiple disciplines [9, 48, 5, 8] are attributed to such scalable intrinsic characteristics and training paradigms. However, corresponding challenges erupt, as multiple rounds of communication of massive model parameters across multi-device clusters have created a significant communication bottleneck in training process. For example, pre-training a BERT-Large model (340M parameters) with a single batch size on 16 GPUs shows that 92% of the training time is spent on gradient all-reduce in backward propagation [49]. Therefore, a critical problem urgently to be addressed is how to relieve the communication burden while ensuring the quality of model training.

In response to the aforementioned problem, a variety of gradient compression strategies have been proposed to reduce the communication overhead of gradients between devices. Such strategies can be broadly categorized into two compression techniques, including low-precision compressors (e.g., SignSGD [6], 1-bit Adam [49] and 1-bit LAMB [29]) and low-rank compressors (e.g., Atomo [57] and PowerSGD [55]). Moreover, error-feedback technique [46, 49, 29] focuses on compensating for errors accumulated during compression by changing the objects to compress from the gradient to the gradient and historical error summation [49, 29]. Error-feedback-based compression algorithms have been theoretically proven to have lower communication complexity when applied to SGD-Type optimizers [53, 30, 18].

However, from the system perspective, how to mitigate communication overhead in practice remains a core problem and a formidable challenge. For example, low-bit gradients (e.g., less than 8-bit) are not supported by typical hardware. Thus, quantizing gradients into less than 8 bits can lead to significant precision loss and numerical instability. For biased low-precision compressors with error-feedback techniques, which do not support communication primitive

054 all-reduce due to their inherent structures, they must use all-gather for aggregation. It
 055 limits them only suitable for master-server communication patterns, incompatible with
 056 advanced ring-based and tree-based patterns in current large-scale model training [38] and
 057 extremely slows down the communication speed [1]. Therefore, there remains a significant
 058 gap between the performance of these methods in training practice and their theoretical
 059 results. Considering the system-level speed, recent studies [1, 59] indicate that when training
 060 representative LLMs with off-the-shelf DistributedDataParallel (DDP), most of gradient
 061 compressors show longer wall-clock training time than vanilla Adam. Furthermore, integrating
 062 these gradient compressors into commonly used optimizers often requires significant
 063 modifications, necessitating additional effort to ensure compatibility and maintain effective.

064 These system-level limitations drive us to consider improvements at the methodological
 065 level. The ineffectiveness of these methods stems from inherent flaws in their methodology.
 066 Specifically, these algorithms seldom take the characteristics of the gradient of LLMs into
 067 account, leading to additional computation or communication rounds to compensate for
 068 the errors introduced by compression. For low-precision compressors, the compression ratio
 069 is upper bounded by floating-point digit number 32. Worse, vector-wise quantization is
 070 independent of the properties of the gradient and is commonly computationally heavy.
 071 Several low-rank compressors [55] consider the low-rank approximation of gradient, but the
 072 compression and decompression are so complex that the time cost in extra computation
 073 is close to or even larger than the saved communication time cost. Therefore, the design
 074 concept of modern "workable" gradient compression algorithms is that

075 **We should design compression algorithms by leveraging the properties of the**
 076 **model, ensuring the suitability for modern LLMs efficient training ecology, and**
 077 **lightweighting compression and decompression computation to save time.**

078 **Contribution.** In this work, we focus on how to design a universal gradient compression
 079 technique in line with the above concept. We propose SEPARATE, a SimplE low-rank
 080 Projection for grAdient compRession in modern lArge-scale model Training procEss, which
 081 compresses the gradient to arbitrary low-dimension one before communication and then
 082 reconstructs after, no matter what optimizers and training frameworks are used. Instead of
 083 a low-rank approximation estimate of weight matrix for parameter-efficient fine-tuning like
 084 LoRA [22], we stand on the low-rank structure of the gradient itself.

085 The motivation of SEPARATE originally comes from the observation of geometric properties
 086 of the Hessian spectrum during training dynamic. Especially, many studies reveal that
 087 the eigen-spectrum of Hessian is often "top-heavy" [55, 43, 44], indicating that several top
 088 eigenvalues are dominant the trace of Hessian. This fact intuitively suggests the theoretical
 089 feasibility of low-rank gradient compression with restricted variance through careful designed
 090 compression strategy. We show the existence of such low-rank properties in Section 3, and
 091 the theoretical validity of SEPARATE in Section 5.

092 Let us give a general introduction to SEPARATE to illustrate its effectiveness. Considering
 093 gradient $\mathbf{g} \in \mathbb{R}^d$ to communicate, we generate a common Gaussian random matrix $\mathbf{M} \in \mathbb{R}^{d \times m}$
 094 on each node and do $\mathbf{p} = \mathbf{g} \times \mathbf{M}$ to compress \mathbf{g} . After communication, we use the same random
 095 matrix for decompression $\tilde{\mathbf{g}} = \mathbf{p} \times \mathbf{M}^\top$. Considering that $\mathbb{E}[\frac{1}{m}\mathbf{p}\mathbf{M}\mathbf{M}^\top] = \mathbf{p}\mathbb{E}[\frac{1}{m}\mathbf{M}\mathbf{M}^\top] = \mathbf{p}$,
 096 we show the compressor is unbiased, and the compression ratio m is arbitrary. Moreover,
 097 the variance analysis seems to be more important. We show theoretically that the variance
 098 is bounded in Section 4, and the gradient complexity for SGD and Adam-Type optimizers
 099 maintains the same order as vanilla SGD and Adam in Section 5.

100 We demonstrate that SEPARATE works well in both LLMs pre-training and fine-tuning tasks.
 101 To reduce compression error in training process, we design a novel error-feedback mechanism
 102 for SEPARATE. We estimate more stable compression errors using a moving average of
 103 historical errors and incorporate these errors back into the gradient before compression. We
 104 also reset the error periodically to eliminate bad historical information and select update
 105 directions precisely. For GPT-2 [40] pre-training, SEPARATE can improve the training
 106 speed of Adam by $2\times$ times. For LLAMA2 [51] fine-tuning, SEPARATE can obtain better
 107 performance on downstream tasks.

108 As a gradient projection method, SEPARATE is independent of the choice of optimizers and
 109 can be regarded as a plug-in, which can be simply implemented with a few lines of code in
 110 off-the-shelf frameworks as shown in Algorithm 2. In addition, the method is robust to some
 111 extent, and its performance is insensitive to the selection of hyperparameters. As long as
 112 the selection of compression ratio meets the random direction sampling quantity required in
 113 theoretical analysis, the algorithm can show effective performance.

114

115

2 RELATED WORK

117

118 **Communication Efficient Training.** As the scale of models explosively grows in recent
 119 years [48, 36, 25, 52], the redundant communication of gradient has become the main
 120 bottleneck of training. Gradient compression [29, 55, 49, 46, 56, 34] is a promising solution
 121 for communication-efficient training among GPUs clusters. In general, the compression
 122 techniques can be divided into low-precision methods [49, 29, 46, 34] and low-rank methods
 123 [55, 32, 2]. Besides, several theoretical and empirical analyses of more general unbiased
 124 compressor \mathcal{C} [18, 53, 21] are also proposed to show the effect of gradient compression
 125 theoretically. Moreover, ZeRO++ [56] has been proposed to apply quantization techniques
 126 to sharding strategy [41].

127

128 **Error-feedback Technique.** Gradient compression techniques bring information loss
 129 during the training process and impair the training accuracy and performance of the model.
 130 The accumulation of error may cause algorithm divergence [46]. To solve such a problem,
 131 the error-feedback technique was first proposed by [46], which adds the compression error to
 132 the gradient before compression in this iteration. Afterward, various works study the effect
 133 of the error feedback technique from theory to practical methods. Recent works [18, 53]
 134 study the theoretical convergence of unbiased compressor \mathcal{C} with error-feedback technique
 135 on convex and non-convex settings. Moreover, many induce the error-feedback technique to
 136 adaptive gradient algorithms[27, 15] which is commonly used in training of large models,
 137 such as 1-bit Adam [49] and 0/1 Adam [34].

138

139 **Low-rank Approximation.** Many studies focus on the low-rank approximation of weight
 140 or gradient matrix in neural network training dynamic and propose the error bound [55,
 141 22]. However, such a low-rank approximation of weight (e.g., LoRA [22]) may not reach
 142 a comparable performance as full-rank in pre-training [31] and fine-tuning [58]. Some
 143 studies show that the Hessian in deep neural networks is "top-heavy" [43, 33, 44], which
 144 means the eigenvalue drops fast and the Hessian maintains low-rank, and some recent
 145 studies theoretically illustrate that the gradient is naturally low-rank [13, 60]. In fact, some
 146 classical methods have considered low-rank estimation of trace, like the Hutchinson estimator
 147 [23]. Such related works provide the potential to design a simple gradient compression
 148 by low-rank projection with restricted variance. Some recent research about training or
 149 gradient accumulation consider the low-rank property of gradient or Hessian, and use random
 150 projection for memory reduction [64, 19], but lack deep analysis on bounded variance.

151

3 LOW-RANK PROPERTY OF GRADIENT AND HESSIAN IN TRAINING

152

153 Through some phenomena observed in practice and simple theoretical analysis of Transformer
 154 [54], we further illustrate the widespread existence of the low-rank property of gradient.
 155 Moreover, we also demonstrate that the eigen-spectrum of Hessian is "top-heavy", consistent
 156 with some previous work about Hessian spectrum of neural networks [43, 44]. We study
 157 these observations practically in this work. As shown in Figure 1, the landscape of gradient
 158 in representative LLMs training possesses low-rank property. Specifically, We observe the
 159 spectrum of GPT-2-Small (125M, with 12 Transformer-based layers) and GPT-2-Medium
 160 (345M, with 24 Transformer-based layers). We observe the gradient spectrums of attention
 161 and MLP in middle layer and last layer, respectively. The eigenvalues of grad drop fast,
 especially in **MLP** layers. This phenomenon is more pronounced in larger models. Based
 162 on recent study on Transformer's dynamic [50], we theoretically prove that the gradient of
 163 MLP layer in Transformer shows low-rank property over time in Appendix D.

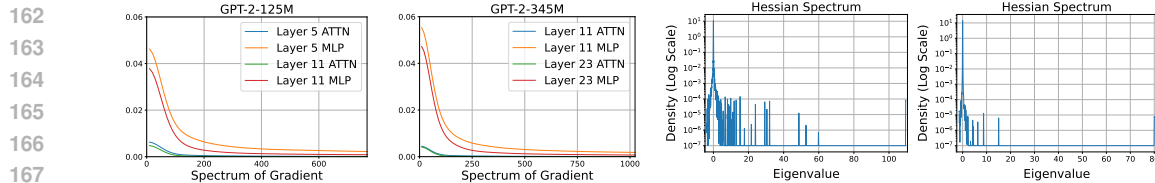


Figure 1: Low-rank gradient and Hessian observations in practice. The two pictures on the left show the spectrum of gradient matrices of chosen layers in GPT-2-125M and GPT-2-345M respectively. The X-axis represents the order of eigenvalues from largest to smallest, and the Y-axis represents the magnitude of eigenvalues. The two pictures on the right show the spectrum of Hessian in ResNet-20 and ResNet-110 trained on CIFAR-10 respectively. The X-axis represents the eigenvalue, and the Y-axis represents the corresponding density.

Algorithm 1 SEPARATE: A Simple Low-rank Projection for Gradient Compression

Require: Initialization model parameters, N nodes, one-round communication budget m , error reset frequency T , $\beta \in [0, 1]$, a common Gaussian random number generator, initialize $\mathbf{e}^0 \in \mathcal{B}(\mathbf{0}, c_1)$

while $k \leq K$ **do**

- STEP 1. In each node n compute stochastic gradient \mathbf{g}_n^k and $\mathbf{h}_n^k = \mathbf{g}_n^k + \mathbf{e}_n^k$;
- STEP 2. Generate fresh i.i.d. common random Gaussian vectors $\xi_1, \dots, \xi_m \sim N(0, \mathbf{I}_d)$ and compute $[p_{1,n}, \dots, p_{m,n}]$ with $p_{i,n} = \langle \mathbf{h}_n^k, \xi_i \rangle$ as the low-dimension projection of \mathbf{h}_n^k ;
- STEP 3. Do all-reduce and obtain global projected gradient $[\tilde{p}_1, \dots, \tilde{p}_m]$;
- STEP 4. Compute $\tilde{\mathbf{h}}_n^k = \frac{1}{m} \sum_{i=1}^m \tilde{p}_i \cdot \xi_i$ and use $\tilde{\mathbf{h}}_n^k$ for model weight update in node n ;
- STEP 5. Update error $\mathbf{e}_n^{k+1} = (1 - \beta)\mathbf{e}_n^k + \beta(\mathbf{h}_n^k - \tilde{\mathbf{h}}_n^k)$ if $k \% T \neq 0$, or $\mathbf{e}_n^{k+1} = 0$ if $k \% T = 0$ (error reset);

end while

Moreover, we study the spectrum of Hessian of trained deep neural networks. In fact, early studies [43] have discovered that the eigenvalues of simple networks (e.g., 3-layer networks) drop fast. As shown in Figure 1, we study the spectrums of Hessian of different scales of ResNet [20] trained on CIFAR-10 [3]. Except several extremely large eigenvalues, most of eigenvalues of the Hessian are close to zero. It is more obvious in larger network structures. This means that a lot of the directions along the loss are almost flat, and the trace of Hessian is bounded much less than $\mathcal{O}(d)$, which ensures our theoretically analysis in Section 5.

4 SEPARATE: A SIMPLE LOW-RANK PROJECTION

Considering low-rank property of gradient and "top-heavy" observation of Hessian, a natural idea of gradient compression is to randomly project the gradient to low-dimensional subspace. As the sample is up to a certain level (usually much less than dimension d), the dominant information of gradient can be exactly recovered. This leads to our SEPARATE method. The core idea of SEPARATE is composed with two parts. First, we design a Gaussian random projection compressor for dimensionality reduction of gradient. Hessian-trace-bounded proposes the theoretical guarantee for random projection. Second, to solve the critical challenge that the compression error in gradient compression would accumulate during the training process, we propose a novel moving average error feedback technique to ensure practical utility. We introduce SEPARATE method in Algorithm 1.

4.1 COMMON RANDOM PROJECTION COMPRESSOR

For classic multi-node parallel training, each node computes its local stochastic gradient \mathbf{g}_n^k with their mini-batch data. Then through communication like all-reduce each node obtains the global gradient for model update.

As mentioned early, we take the low-rank property of gradient and "top-heavy" property of Hessian into account to design a variance-bounded low-rank projection for gradient compression, applicable to most of practical scenarios in large-scale model training. Specifi-

cally, for the gradient vector \mathbf{g} , each node generates m common random Gaussian variables $\xi_1, \dots, \xi_m \sim N(0, \mathbf{I}_d)$. Then each node computes

$$p_i = \langle \mathbf{g}, \xi_i \rangle, \forall i \in [m]. \quad (1)$$

After compression, each node constructs $[p_1, \dots, p_m]$ as the compressed gradient for communication like all-reduce. Then they obtain the global $[\tilde{p}_1, \dots, \tilde{p}_m]$, and reconstruct the gradient as

$$\tilde{\mathbf{g}} = \frac{1}{m} \sum_{i=1}^m \tilde{p}_i \cdot \xi_i. \quad (2)$$

Then we theoretically illustrate the unbiasedness and variance-bounded property of our common random projection in Lemma 4.1 and Lemma 4.2 as below. The proof details are shown in Appendix B.

Lemma 4.1. $\tilde{\mathbf{g}}$ is an unbiased estimator of \mathbf{g} ,

$$\mathbb{E}_{\xi_1, \dots, \xi_m} \tilde{\mathbf{g}} = \mathbf{g}. \quad (3)$$

Lemma 4.2. The variance of $\tilde{\mathbf{g}}$ under norm $\|\cdot\|_{\mathbf{A}}$, where \mathbf{A} is a given positive semi-definite symmetric matrix, can be bounded by $\frac{3\text{tr}(\mathbf{A})}{m} \|\mathbf{g}\|^2 - \frac{1}{m} \|\mathbf{g}\|_{\mathbf{A}}^2$,

$$\mathbb{E}_{\xi_1, \dots, \xi_m} \|\tilde{\mathbf{g}} - \mathbf{g}\|_{\mathbf{A}}^2 \leq \frac{3\text{tr}(\mathbf{A})}{m} \|\mathbf{g}\|^2 - \frac{1}{m} \|\mathbf{g}\|_{\mathbf{A}}^2. \quad (4)$$

Remark 4.3. Lemma 4.1 directly indicates the unbiasedness of common random projection, which is standard for low-rank compression techniques [55, 64, 19]. What we really highlight is Lemma 4.2, which illustrate that the variance of our compression strategy under the Mahalanobis norm can be bounded by the trace of given matrix. Considering the standard convergence analysis of SGD or Adam-Type optimizers, the second order factor of Taylor expansion of the objective function can be written as Mahalanobis norm under Hessian matrix, and the "top-heavy" property ensures the trace of Hessian is much smaller than dL , where d is the dimension and L is Lipschitz constant defined in Assumption 5.2. This provides the potential for SEPARATE-based algorithms to surpass other compressors in the order of d in convergence speed. We show the theoretical results in Section 5.

4.2 MOVING AVERAGE ERROR FEEDBACK

Error-feedback technique is widely used in gradient compression methods [46, 42] to mitigate the information loss during compression. It is worth considering how error-feedback works for our common random projection compressor, even though Lemma 4.1 and Lemma 4.2 show the unbiasedness and trace-bounded variance, because the accumulated error in continuous updates may cause wide deviation. One straight solution is to use the gradient compression error from the previous iteration as $\mathbf{e}_n^k = \arg \min_{\mathbf{e} \in \mathbb{R}^d} \left\| \mathbf{e} - (\tilde{\mathbf{h}}_n^k - \mathbf{g}_n^k) \right\|^2 = \tilde{\mathbf{h}}_n^k - \mathbf{g}_n^k$, where \mathbf{g}_n^k is the original gradient on the n -th node and $\tilde{\mathbf{h}}_n^k$ is the reconstruction of compressed gradient. However, we empirically discover the instability of this estimate, because for single-step iteration, random vectors for projection may have a large deviation from the direction of true gradient. This means potential abrupt fluctuations of \mathbf{e}_n^k , especially for several continuous iterations with a series of random vectors with very different directions. This may lead to the whole training process converging to another suboptimal region. This phenomenon is particularly prominent when training from scratch, changing the shape of loss curve and the convergence result of loss (see Section 6.3). To solve this problem, inspired by the idea of momentum technique in the analyses of accelerated gradient descent [37], we take the moving average of the historical compression error and the current one to maintain the continuity to some degree:

$$\mathbf{e}_n^k = \operatorname{argmin}_{\mathbf{e} \in \mathbb{R}^d} \frac{\beta}{2} \left\| \mathbf{e} - (\tilde{\mathbf{h}}_n^k - \mathbf{g}_n^k) \right\|^2 + \frac{1-\beta}{2} \left\| \mathbf{e} - \mathbf{e}_n^{k-1} \right\|^2 = (1-\beta) \mathbf{e}_n^{k-1} + \beta (\tilde{\mathbf{h}}_n^k - \mathbf{g}_n^k), \quad (5)$$

where $\beta \in [0, 1]$ represents the trade-off between two factors. We demonstrate that the moving average error feedback can reduce the total accumulated error when applying it

270 to SGD or Adam-Type optimizers in Lemma C.2 and Lemma C.3. In brief, we simply
 271 formulate the iteration of SGD and Adam-Type optimizers as $\boldsymbol{\theta}^k = \boldsymbol{\theta}^0 - \sum_{i=i}^k \boldsymbol{\eta}^i \circ \mathbf{g}^i$, where
 272 $\boldsymbol{\theta}$ means the model's weight and \circ means the Hadamard product of two vectors. Our analysis
 273 shows that moving average error-feedback effectively reduces the accumulated gap of weights
 274 updated by \mathbf{g} and by $\tilde{\mathbf{g}}$ as
 275

$$\left\| \sum_{i=i}^k \boldsymbol{\eta}^i \circ \mathbf{g}^i - \sum_{i=i}^k \boldsymbol{\eta}^i \circ \tilde{\mathbf{g}}^i \right\| \leq \mathcal{O}(\eta \|\mathbf{e}^k\|), \quad (6)$$

276 which means as the training goes on, the accumulated compression error of the top k rounds
 277 is only of \mathbf{e}^k -order, instead of the accumulation from \mathbf{e}^0 to \mathbf{e}^k . Compared with vanilla error
 278 feedback technique [46], taking moving average of the historical error maintains stability to
 279 some extent and reduces the variance of accumulated error.
 280

281 Moreover, we consider the compression error in the early training process cannot guide the
 282 later iteration, so we reset the compression error after a given number of iterations like
 283 128. Combining the techniques above we propose SEPARATE method in Algorithm 1. Our
 284 SEPARATE can be applied to all the gradient-based optimizers with a few lines of codes, as
 285 shown in Algorithm 2.
 286

288 5 CONVERGENCE GUARANTEE

290 In this section, we propose the convergence guarantee of our SEPARATE method. We
 291 consider the following non-convex optimization problem
 292

$$\min_{\boldsymbol{\theta}} f(\boldsymbol{\theta}) = \mathbb{E}_{\zeta \sim \mathcal{D}} [F(\boldsymbol{\theta}, \zeta)], \quad (7)$$

293 where F is the non-convex optimization objective and $\boldsymbol{\theta}$ is the model weight to update. Data
 294 is sampled from a given distribution \mathcal{D} . We focus on the convergence rate of SEPARATE-
 295 based SGD and Adam-Type Optimizer to find an ϵ -approximate first-order stationary point
 296 of the objective $f(\cdot)$. For such SEPARATE-based optimizers, they update the model weight
 297 as below:
 298

$$\text{SGD : } \boldsymbol{\theta}^{k+1} = \boldsymbol{\theta}^k - \eta \tilde{\mathbf{h}}^k, \quad \text{Adam-Type : } \begin{cases} \mathbf{m}^k = (1 - \beta_1) \mathbf{m}^{k-1} + \beta_1 \tilde{\mathbf{h}}^k, \\ \boldsymbol{\eta}^k = \eta \times v(\tilde{\mathbf{h}}^0, \dots, \tilde{\mathbf{h}}^k), \\ \boldsymbol{\theta}^{k+1} = \boldsymbol{\theta}^k - \boldsymbol{\eta}^k \circ \mathbf{m}^k, \end{cases} \quad (8)$$

300 where $\beta_1 \in (0, 1)$, and $v(\cdot)$ computes a series of pre-conditioners based on different AdamType
 301 optimizers. For example, $v(\cdot)$ computes the inverse of the second order moment of Adam's
 302 gradient like $v(\tilde{\mathbf{h}}^0, \dots, \tilde{\mathbf{h}}^k) = 1/\sqrt{\mathbf{v}^k + \delta}$ where $\mathbf{v}^k = (1 - \beta_2) \mathbf{v}^{k-1} + \beta_2 (\tilde{\mathbf{h}}^k)^2$. Adam-Type
 303 optimizers differ from various definitions of $v(\cdot)$ [27, 15, 47]. We analyze them uniformly.
 304

305 Like the common analysis of the convergence rate of general non-convex objective [24], we
 306 define the ϵ -approximate first-order stationary point as below.
 307

308 **Definition 5.1** (ϵ -stationary point). *The model weight $\boldsymbol{\theta}$ is an ϵ -approximate first-order
 309 stationary point of f if $\|\nabla f(\mathbf{x})\| \leq \epsilon$.*
 310

311 Definition 5.1 means for SGD and Adam-Type optimizers, we need to find the iteration
 312 round K such that $\min_{k \in [K]} \mathbb{E} \|\nabla f(\boldsymbol{\theta}^k)\| \leq \epsilon$, or more tightly
 313

$$\frac{1}{K} \sum_{k=0}^{K-1} \mathbb{E} \|\nabla f(\boldsymbol{\theta}^k)\|^2 \leq \epsilon^2. \quad (9)$$

314 Moreover, we formally present some assumptions to constrain the objective function and the
 315 optimization problem. Assumption 5.2 and 5.3 are commonly used to describe the properties
 316 of the objective in stochastic setting [24, 16]. Assumption 5.4 ensures the trace of Hessian is
 317 bounded globally, which is also common in practical applications [43].
 318

319 **Assumption 5.2** (L-smoothness). *The function f is L-smooth if it satisfies*
 320

$$\|f(\boldsymbol{\theta}_1) - f(\boldsymbol{\theta}_2)\| \leq L \|\boldsymbol{\theta}_1 - \boldsymbol{\theta}_2\|, \quad \forall \boldsymbol{\theta}_1, \boldsymbol{\theta}_2 \in \mathbb{R}^d. \quad (10)$$

Assumption 5.3 (Stochastic Gradient Boundness). *The stochastic gradient \mathbf{g}^k on each device is unbiased and its infinite norm and variance are bounded as:*

$$\mathbb{E}\|\mathbf{g}^k\|_\infty \leq c_\infty, \quad \mathbb{E}\|\nabla f(\boldsymbol{\theta}^k) - \mathbf{g}^k\|^2 \leq \sigma^2, \quad \forall k \in [K]. \quad (11)$$

Assumption 5.4 (Hessian-domination). *The function f is \mathbf{A} -Hessian dominated if there exists a matrix \mathbf{A} such that $\nabla^2 f(\boldsymbol{\theta}) \preceq \mathbf{A}, \forall \boldsymbol{\theta} \in \mathbb{R}^d$.*

Now we present the main theorem of the convergence rate of SEPARATE-based SGD and Adam-Type optimizers in general non-convex setting. The proof of two Theorems can be seen in Appendix C.

Theorem 5.5 (SEPARATE-based SGD convergence). *Suppose Assumption 5.2, 5.3 and 5.4 hold. Let $\mathbf{e}^0 \in \mathcal{B}(\mathbf{0}, c_1)$, namely $\forall \mathbf{x} \in \mathcal{B}(\mathbf{0}, c_1), \|\mathbf{x}\| \leq c_1$. Let $m \leq \frac{\text{tr}(\mathbf{A})}{L}$ and $\eta \leq \frac{m}{4\text{tr}(\mathbf{A})}$. With $\eta = \mathcal{O}(d^{-1/2}\epsilon^2)$ in SEPARATE-based SGD, after $K = \Omega(d^{1/2}\epsilon^{-4})$ iterations in Algorithm 1, it holds*

$$\frac{1}{K} \sum_{k=0}^K \mathbb{E} \left\| \nabla f(\tilde{\boldsymbol{\theta}}^k) \right\|^2 \leq \mathcal{O}(\epsilon^2). \quad (12)$$

Remark 5.6. *This improved convergence rate under standard non-convex stochastic setting is derived from our analysis of trace-bounded variance in Lemma 4.2. In the common analysis of compression techniques, compression reduces the amount of information through single step communication by $\mathcal{O}(d)$ times, or with $\mathcal{O}(d)$ -variance [2]. Moreover, considering error feedback technique brings bias, the analysis is commonly element-wise [2, 46]. Thus the convergence rate is often dimensional dependent $\mathcal{O}(d\epsilon^{-4})$, but they assume it is default and usually ignore this item [46]. Considering modern LLMs training, the dimension of parameters is often extremely large and cannot be ignored. Fortunately, our analysis provides an improved rate on the order of d from $\mathcal{O}(d)$ to $\mathcal{O}(d^{1/2})$ under natural defined Assumption 5.3 from "top-heavy" Hessian observation. It is the first gradient compression method to achieve such rate to the best of our knowledge.*

Theorem 5.7 (SEPARATE-based Adam-Type convergence). *Suppose Assumption 5.2, 5.3 hold. Assume $c_l \leq \|v(\cdot)\|_\infty \leq c_u$ and $\|\boldsymbol{\eta}^k - \boldsymbol{\eta}^{k-1}\|_\infty \leq \eta \beta_1 (1 - \beta_1)^{K-k} c_u$. Let $\mathbf{e}^0 \in \mathcal{B}(\mathbf{0}, c_1)$, $\eta \leq \min\left\{\frac{c_l}{2Lc_u^2}, \frac{\beta_1 c_l^{0.5}}{5c_u^{1.5}(1-\beta_1)L}\right\}$. With $\eta = \mathcal{O}(d^{-1}\epsilon^2)$ and $\beta_1 = \mathcal{O}(d^{-1}\epsilon^2)$ in SEPARATE-based Adam-Type optimizers, after $K = \Omega(d\epsilon^{-4})$ iterations in Algorithm 1, it holds*

$$\frac{1}{K} \sum_{k=0}^{K-1} \mathbb{E} \left[\left\| \nabla f(\tilde{\boldsymbol{\theta}}^k) \right\|^2 + \frac{1}{4} \left\| \mathbf{m}^k \right\|^2 \right] \leq \mathcal{O}(\epsilon^2). \quad (13)$$

Remark 5.8. *Because different coordinates of the gradient are updated with different step sizes in Adam-Type optimizers, the convergence rate is inevitably dependent on dimension d , and combined with compression and error feedback, Adam-Type optimizers are often $\mathcal{O}(d)$ at the order of d . Theorem 5.7 shows that integrating SEPARATE with various Adam-Type optimizers does not affect their convergence speed. Thus SEPARATE-based Adam-Type optimizers share the same stochastic gradient complexity as $\mathcal{O}(\epsilon^{-4})$ when ignoring the dimensional factor d .*

6 EXPERIMENTS

6.1 SOTA COMPARISON WITH COMMUNICATION EFFICIENT METHODS

We evaluate SEPARATE on both pre-training and fine-tuning tasks of LLMs. The experiment setting details are shown in Appendix E.

Pre-Training GPT-2 from Scratch. We train GPT-2-345M with vanilla Adam optimizer as a baseline and compare the convergence speed with our SEPARATE-based Adam optimizer with baseline and PowerSGD [55]. We set different compression ratios of SEPARATE and compare the convergence speed of iteration steps and wall-clock time, respectively in Figure 2 (a) and (b). Figure 2 (a) demonstrates that though high compression ratio results in more

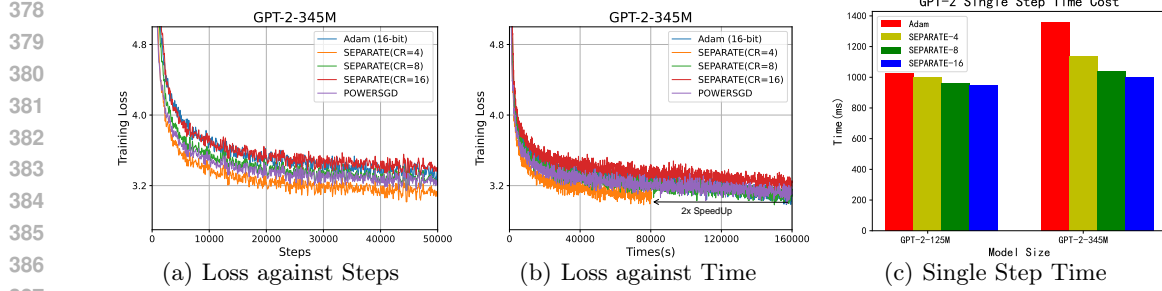


Figure 2: Loss curve and single step time cost of vanilla Adam and SEPARATE with different compression ratios (CR) on GPT-2-345M trained with 50B tokens OpenWebtext dataset. (a) shows the loss against the iteration steps, and (b) shows the loss against the wall-clock time. (c) shows the single-step time cost of vanilla Adam and SEPARATE with different compression ratios.

Table 1: Performance comparison with representative communication-efficient methods. We fine-tune LLAMA2-7B on the alpaca-gpt4 dataset and evaluate the performance on downstream tasks, including commonsense reasoning, world knowledge, math, and code.

| Method | TriQA | GSM8K | MBPP | NQ | WinoG | Arc-e | Arc-c | PIQA | HellaS | Avg.S | Avg.R |
|------------|--------------|--------------|--------------|-------------|--------------|--------------|--------------|--------------|--------------|--------------|-------------|
| Adam | 49.39 | 15.69 | 19.40 | 3.07 | 46.09 | 72.31 | 53.90 | 57.07 | 26.45 | 38.15 | 3.22 |
| PowerSGD | 50.78 | 18.65 | 22.40 | 2.52 | 40.57 | 62.43 | 42.71 | 52.88 | 30.12 | 35.90 | 3.00 |
| 1-bit Adam | 62.08 | 16.53 | 16.80 | 5.15 | 49.57 | 49.21 | 37.97 | 52.88 | 22.04 | 34.69 | 3.22 |
| ZeRO++ | 57.49 | 18.42 | 22.20 | 1.72 | 49.88 | 43.03 | 30.85 | 47.61 | 33.97 | 33.91 | 3.22 |
| SEPARATE | 57.18 | 20.17 | 21.40 | 4.18 | 49.25 | 72.66 | 49.83 | 52.99 | 29.73 | 39.71 | 2.22 |

steps to reach the same loss, SEPARATE-based optimizer with the proper compression ratio even has a faster convergence speed of iteration steps. Figure 2 (b) shows that SEPARATE can accelerate the training speed up to $2\times$ for GPT-2-345M pre-training by trade-off the compression ratio and one-step cost, compared with baseline and PowerSGD. Thus we think effective designing algorithms based on low-rank gradient and Hessian of model ensures accurate training with lower cost. Moreover, we test the single-step time cost of vanilla Adam and SEPARATE with different compression ratios on GPT-2-125M and GPT-2-345M. We find that when model scale increases, the effect of SEPARATE is more remarkable, so SEPARATE is significant in training large-scale models.

Fine-tuning LLAMA2 and Evaluating on Downstream Tasks. We follow Llama-Accessory [63] and fine-tune LLAMA2-7B[51] model on alpaca-gpt4 [39] dataset for three epochs, and evaluate the ability of fine-tuned model on several downstream tasks including commonsense reasoning, world knowledge, math and code. We report the scores obtained on these evaluation benchmarks in Table 1. We compute the average score (Avg.S, \uparrow) and average rank (Avg.R, \downarrow) of each method. The results indicate that SEPARATE outperforms other low-rank or low-bit optimizers with error feedback and ZeRO++, even beyond the performance of vanilla Adam optimizer without compression on the comprehensive performance of all the downstream tasks. Moreover, other communication-efficient optimizers have much worse performance than SEPARATE and vanilla Adam, especially on commonsense reasoning tasks. The possible reason for this result is that their last-iteration-based error feedback cannot deal with the accumulated error during the whole process, while SEPARATE is applied with the moving average of the historical error to stabilize the error and error reset mechanism to remove useless information.

6.2 ABLATION EXPERIMENTS

We conduct ablation experiments to explore the effect of each component in SEPARATE, including 1)error-feedback technique (Err.Fed.), 2)moving average update of error (Err.Avg.) and 3)error reset mechanism (Err.Re.). For training from scratch, without error-feedback and moving average techniques, the training process becomes unstable and cannot converge. We show the results in Section 6.3. For fine-tuning tasks, we fine-tune the LLAMA2-7B model on alpaca-gpt4 dataset, applying SEPARATE on Adam optimizer with bfloat16 precision. The results are shown in Table 2.

432

433 Table 2: Effects of components in SEPARATE to the performance of LLAMA2-7B fine-tuned
 434 on alpaca-gpt4 dataset, including error-feedback technique (Err.Fed.), moving average on
 435 error (Err.Avg.) and error reset mechanism (Err.Re.).

| Method | Err.Fed. | Err.Avg. | Err.Re. | GSM8K | MBPP | NQ | Arc-e | Arc-c | PIQA | Avg. |
|-----------|----------|----------|---------|--------------|--------------|-------------|--------------|--------------|--------------|--------------|
| SEPARATE1 | False | N/A | N/A | 21.53 | 22.00 | 4.57 | 71.25 | 49.15 | 52.61 | 36.86 |
| SEPARATE2 | True | False | N/A | 20.17 | 21.80 | 4.35 | 69.14 | 51.19 | 52.29 | 36.49 |
| SEPARATE3 | True | True | N/A | 20.92 | 22.00 | 4.49 | 69.49 | 51.53 | 52.23 | 36.77 |
| SEPARATE4 | True | True | 512 | 20.39 | 21.40 | 4.46 | 70.02 | 49.49 | 52.45 | 36.37 |
| SEPARATE5 | True | True | 128 | 20.17 | 21.40 | 4.18 | 72.66 | 49.83 | 52.99 | 36.87 |

441

442 Table 3: Effect of different compression ratios of SEPARATE to the performance of LLAMA2-
 443 7B fine-tuned on alpaca-gpt4 dataset, where SEPARATE-X means we set the compression
 444 ratio at X.

| Method | TriQA | GSM8K | MBPP | NQ | WinoG | Arc-e | Arc-c | PIQA | HellaS | Avg. |
|--------------|--------------|--------------|--------------|-------------|--------------|--------------|--------------|--------------|--------------|--------------|
| SEPARATE-8 | 55.43 | 18.88 | 21.00 | 4.13 | 45.78 | 74.07 | 50.85 | 52.83 | 32.43 | 39.49 |
| SEPARATE-16 | 57.18 | 20.17 | 21.40 | 4.18 | 49.25 | 72.66 | 49.83 | 52.99 | 29.73 | 39.71 |
| SEPARATE-64 | 59.00 | 19.03 | 20.40 | 4.54 | 49.8 | 68.43 | 48.47 | 52.88 | 28.59 | 39.02 |
| SEPARATE-128 | 58.93 | 18.65 | 22.40 | 4.79 | 50.28 | 65.78 | 47.46 | 52.67 | 27.79 | 38.75 |

449

450 **Error-feedback Technique.** We first study the effect of directly applying the vanilla
 451 error-feedback technique on the common random projection compressor of SEPARATE.
 452 Comparing SEPARATE1 with SEPARATE2, we can observe that directly applying error-
 453 feedback technique even slightly impairs the whole fine-tuning performance, especially on
 454 commonsense reasoning tasks such as WinoG, Arc and PIQA. This may be due to the
 455 randomness of projection directions. When the random projection directions are far from
 456 the dominant directions of Hessian in several continuous iterations, the variance of error will
 457 become extremely large and misguide the next iteration. Thus we need another technique to
 458 smooth errors and drop the misleading information arising from randomness.

459 **Moving Average Update of Error.** We use the moving average of the historical error and
 460 the current one to replace the direct error from the last iteration, to reduce the instability
 461 of vanilla error-feedback technique. Comparing SEPARATE2 and SEPARATE3 we can
 462 find that the moving average update of error improves the whole fine-tuning performance,
 463 especially on Arc-c and MBPP tasks. However, because of the randomness of the compressor,
 464 the accumulated misleading information of inexact directions still impairs the performance
 465 compared with SEPARATE1.

466 **Error Reset Mechanism.** We notice that random projection may generate bad directions
 467 far away from the dominant ones of Hessian even with unbiased estimate. Especially
 468 compared with quantization methods some bad projections may cause extremely large error.
 469 To solve the accumulated bad random information arising from the random projection in the
 470 compression error, we design error reset mechanism to reset the accumulated error frequently.
 471 Comparing SEPARATE3, SEPARATE4 and SEPARATE5, we find that the appropriate
 472 set of error reset frequency T can improve the performance, and too large set of error reset
 473 frequency still causes the misleading information accumulation and worse accuracy.

473

474 6.3 HYPER-PARAMETERS CHOICE OF SEPARATE

475

476 **Random Seed Choice of Projection.** In the SEPARATE method, we introduce extra
 477 randomness due to the random projection. Thus in practice we need to set an extra random
 478 seed for commonly generating the same random Gaussian vectors on different devices. In
 479 order to clarify that our method works not depending on the choice of seed, we select different
 480 common random seeds for projection to repeat training GPT-2-350M with compression ratio
 481 16. The results are shown in Figure 3 (a), where we randomly set seed as 3407, 4396 and 37,
 482 and the results make no difference.

483

484 **β in Moving Average of Error.** SEPARATE method introduces an extra hyper-parameter
 485 β for moving average update of error. We tested the effect of β selection on the convergence
 486 speed. We test different β in the first 10000 steps of GPT-2-345M training. The results in
 487 Figure 3 (b) show that SEPARATE is sensitive to the choice of β . If we set $\beta = 1$, which

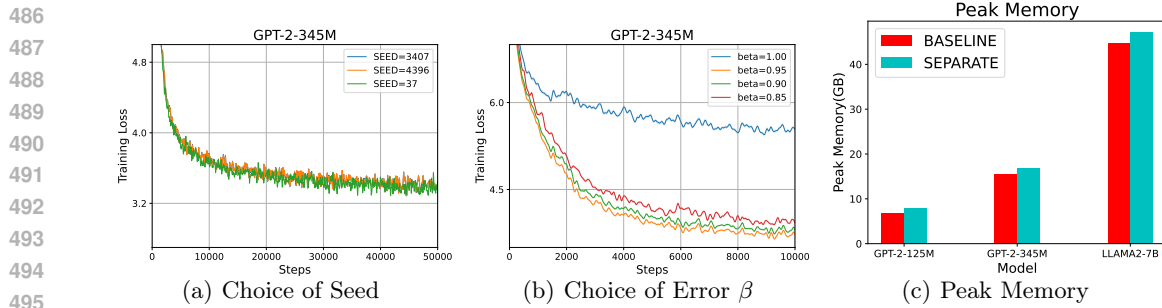


Figure 3: Hyper-parameter choice of SEPARATE and memory cost report. (a) shows the effect of different common random seeds to SEPARATE training with compression ratio 16. (b) shows the effect of different β choices of moving average update of error to SEPARATE training with compression ratio 16. (c) shows the peak memory in Adam and SEPARATE training on different models with compression ratio 16.

means we do not use moving average update of error, the convergence speed shows down remarkably in the first few steps, and in the subsequent iterations it seriously deviates from the optimal dynamic. Setting $\beta = 0.95$ seems to be acceptable, and when decreasing β , the convergence speed slows down again. When $\beta \leq 0.80$, the training dynamic becomes unstable with loss value increasing to NaN, which means that if we gradually ignore the compression error of current iteration, (specifically $\beta = 0$ means we do not use error-feedback technique), the training process becomes unstable and cannot converge.

Compression Ratio. We conduct experiments to test the effect of the scale of compression ratio on the performance of models. One advantage of SEPARATE is that SEPARATE can set the compression ratio by users themselves instead of 4 or 8 (at most 32) like quantization methods. We set the compression ratio as 8, 16, 64, and 128, respectively, and tested the performance of the fine-tuned model on downstream tasks. The results are shown in Table 3. The results show that increasing the compression ratio to a certain extent enhances the performance of the model, due to the certain noise improving the generalization of models. Besides, an overlarge compression ratio reduces the performance of models, but the accuracy loss is within the acceptable range because if we compress the gradient 128 times, the communication cost is a quarter of 1-bit quantization methods and the performance is better than it. We also find that with different compression ratios, SEPARATE focuses on different types of tasks, so users can set the ratio adaptively.

6.4 MEMORY COST OF SEPARATE

We report the peak memory in Figure 3 (c). Results show the peak memory when training or fine-tuning corresponding models, which demonstrates that the extra memory SEPARATE is negligible in comparison with the communication cost it saves. Moreover, by expanding the random vector buffer, we can save time in generating random Gaussian vectors, which means we can use some memory cost to exchange computational time in compression and decompression to accelerate training process.

7 CONCLUSION

In this paper, we propose a simple low-rank projection for gradient compression in modern large-scale model training process named SEPARATE. We have carried out theoretical analysis and a lot of experimental verification to illustrate SEPARATE provides an easy way to apply gradient compression to all types of gradient-based optimizers across various training frameworks, while maintaining high-quality training performance and achieving significant compression. We think SEPARATE is helpful for the further study and popularization of large-scale models.

540 REFERENCES
541

- 542 [1] Saurabh Agarwal et al. “On the utility of gradient compression in distributed training
543 systems”. In: *Proceedings of Machine Learning and Systems* 4 (2022), pp. 652–672.
- 544 [2] Alham Fikri Aji and Kenneth Heafield. “Sparse communication for distributed gradient
545 descent”. In: *arXiv preprint arXiv:1704.05021* (2017).
- 546 [3] Krizhevsky Alex. “Learning multiple layers of features from tiny images”. In:
547 <https://www.cs.toronto.edu/kriz/learning-features-2009-TR.pdf> (2009).
- 548 [4] Jacob Austin et al. “Program synthesis with large language models”. In: *arXiv preprint*
549 *arXiv:2108.07732* (2021).
- 550 [5] Yutong Bai et al. “Sequential modeling enables scalable learning for large vision models”.
551 In: *arXiv preprint arXiv:2312.00785* (2023).
- 552 [6] Jeremy Bernstein et al. “signSGD: Compressed optimisation for non-convex problems”.
553 In: *International Conference on Machine Learning*. PMLR. 2018, pp. 560–569.
- 554 [7] Yonatan Bisk et al. “Piqqa: Reasoning about physical commonsense in natural language”.
555 In: *Proceedings of the AAAI conference on artificial intelligence*. Vol. 34. 05. 2020,
556 pp. 7432–7439.
- 557 [8] Andreas Blattmann et al. “Align your latents: High-resolution video synthesis with
558 latent diffusion models”. In: *Proceedings of the IEEE/CVF Conference on Computer*
559 *Vision and Pattern Recognition*. 2023, pp. 22563–22575.
- 560 [9] Tom Brown et al. “Language models are few-shot learners”. In: *Advances in neural*
561 *information processing systems* 33 (2020), pp. 1877–1901.
- 562 [10] Peter Clark et al. “Think you have solved question answering? try arc, the ai2 reasoning
563 challenge”. In: *arXiv preprint arXiv:1803.05457* (2018).
- 564 [11] Karl Cobbe et al. “Training verifiers to solve math word problems”. In: *arXiv preprint*
565 *arXiv:2110.14168* (2021).
- 566 [12] OpenCompass Contributors. “Opencompass: A universal evaluation platform for foun-
567 dation models”. In: *GitHub repository* (2023).
- 568 [13] Romain Cosson et al. “Low-Rank Gradient Descent”. In: *IEEE Open Journal of Control*
569 *Systems* (2023).
- 570 [14] Ning Ding et al. “Delta tuning: A comprehensive study of parameter efficient methods
571 for pre-trained language models”. In: *arXiv preprint arXiv:2203.06904* (2022).
- 572 [15] John Duchi, Elad Hazan, and Yoram Singer. “Adaptive subgradient methods for online
573 learning and stochastic optimization.” In: *Journal of machine learning research* 12.7
574 (2011).
- 575 [16] Cong Fang, Zhouchen Lin, and Tong Zhang. “Sharp analysis for nonconvex sgd escaping
576 from saddle points”. In: *Conference on Learning Theory*. PMLR. 2019, pp. 1192–1234.
- 577 [17] Aaron Gokaslan and Vanya Cohen. *OpenWebText Corpus*. <http://Skylion007.github.io/OpenWebTextCorpus>. 2019.
- 578 [18] Eduard Gorbunov et al. “MARINA: Faster non-convex distributed learning with com-
579 pression”. In: *International Conference on Machine Learning*. PMLR. 2021, pp. 3788–
580 3798.
- 581 [19] Yongchang Hao, Yanshuai Cao, and Lili Mou. *Flora: Low-Rank Adapters Are Secretly*
582 *Gradient Compressors*. 2024. arXiv: 2402.03293 [cs.LG]. URL: <https://arxiv.org/abs/2402.03293>.
- 583 [20] Kaiming He et al. “Deep residual learning for image recognition”. In: *Proceedings of*
584 *the IEEE conference on computer vision and pattern recognition*. 2016, pp. 770–778.
- 585 [21] Yutong He, Xinneng Huang, and Kun Yuan. “Unbiased Compression Saves Communi-
586 cation in Distributed Optimization: When and How Much?” In: *Advances in Neural*
587 *Information Processing Systems* 36 (2024).
- 588 [22] Edward J Hu et al. “Lora: Low-rank adaptation of large language models”. In: *arXiv*
589 *preprint arXiv:2106.09685* (2021).
- 590 [23] M.F. Hutchinson. “A stochastic estimator of the trace of the influence matrix for Lapla-
591 cian smoothing splines”. In: *Communication in Statistics- Simulation and Computation*
592 18 (Jan. 1989), pp. 1059–1076. DOI: 10.1080/03610919008812866.

- 594 [24] Prateek Jain, Purushottam Kar, et al. “Non-convex optimization for machine learning”.
 595 In: *Foundations and Trends® in Machine Learning* 10.3-4 (2017), pp. 142–363.
- 596 [25] Albert Q Jiang et al. “Mixtral of experts”. In: *arXiv preprint arXiv:2401.04088* (2024).
- 597 [26] Mandar Joshi et al. “Triviaqa: A large scale distantly supervised challenge dataset for
 598 reading comprehension”. In: *arXiv preprint arXiv:1705.03551* (2017).
- 599 [27] Diederik P Kingma and Jimmy Ba. “Adam: A method for stochastic optimization”. In:
 600 *arXiv preprint arXiv:1412.6980* (2014).
- 601 [28] Tom Kwiatkowski et al. “Natural questions: a benchmark for question answering
 602 research”. In: *Transactions of the Association for Computational Linguistics* 7 (2019),
 603 pp. 453–466.
- 604 [29] Conglong Li et al. “1-bit LAMB: communication efficient large-scale large-batch training
 605 with LAMB’s convergence speed”. In: *2022 IEEE 29th International Conference on
 606 High Performance Computing, Data, and Analytics (HiPC)*. IEEE. 2022, pp. 272–281.
- 607 [30] Zhize Li et al. “Acceleration for compressed gradient descent in distributed and federated
 608 optimization”. In: *arXiv preprint arXiv:2002.11364* (2020).
- 609 [31] Vladislav Lalin et al. “Relora: High-rank training through low-rank updates”. In: *The
 610 Twelfth International Conference on Learning Representations*. 2023.
- 611 [32] Yujun Lin et al. “Deep gradient compression: Reducing the communication bandwidth
 612 for distributed training”. In: *arXiv preprint arXiv:1712.01887* (2017).
- 613 [33] Yuanshi Liu et al. *Accelerated Gradient Algorithms with Adaptive Subspace Search for
 614 Instance-Faster Optimization*. 2023. arXiv: 2312.03218 [cs.LG].
- 615 [34] Yucheng Lu et al. “Maximizing communication efficiency for large-scale training via
 616 0/1 adam”. In: *arXiv preprint arXiv:2202.06009* (2022).
- 617 [35] David Luebke. “CUDA: Scalable parallel programming for high-performance scientific
 618 computing”. In: *2008 5th IEEE international symposium on biomedical imaging: from
 619 nano to macro*. IEEE. 2008, pp. 836–838.
- 620 [36] Deepak Narayanan et al. “Efficient large-scale language model training on gpu clus-
 621 ters using megatron-lm”. In: *Proceedings of the International Conference for High
 622 Performance Computing, Networking, Storage and Analysis*. 2021, pp. 1–15.
- 623 [37] Yurii Nesterov. *Introductory lectures on convex optimization: A basic course*. Vol. 87.
 624 Springer Science & Business Media, 2013.
- 625 [38] Pitch Patarasuk and Xin Yuan. “Bandwidth optimal all-reduce algorithms for clusters of
 626 workstations”. In: *Journal of Parallel and Distributed Computing* 69.2 (2009), pp. 117–
 627 124.
- 628 [39] Baolin Peng et al. “Instruction tuning with gpt-4”. In: *arXiv preprint arXiv:2304.03277*
 629 (2023).
- 630 [40] Alec Radford et al. “Language models are unsupervised multitask learners”. In: *OpenAI
 631 blog* 1.8 (2019), p. 9.
- 632 [41] Samyam Rajbhandari et al. “Zero: Memory optimizations toward training trillion pa-
 633 rameter models”. In: *SC20: International Conference for High Performance Computing,
 634 Networking, Storage and Analysis*. IEEE. 2020, pp. 1–16.
- 635 [42] Peter Richtárik, Igor Sokolov, and Ilyas Fatkhullin. “EF21: A new, simpler, theoretically
 636 better, and practically faster error feedback”. In: *Advances in Neural Information
 637 Processing Systems* 34 (2021), pp. 4384–4396.
- 638 [43] Levent Sagun, Leon Bottou, and Yann LeCun. “Eigenvalues of the hessian in deep
 639 learning: Singularity and beyond”. In: *arXiv preprint arXiv:1611.07476* (2016).
- 640 [44] Levent Sagun et al. *Empirical Analysis of the Hessian of Over-Parametrized Neural
 641 Networks*. 2018. arXiv: 1706.04454 [cs.LG]. URL: <https://arxiv.org/abs/1706.04454>.
- 643 [45] Keisuke Sakaguchi et al. “Winogrande: An adversarial winograd schema challenge at
 644 scale”. In: *Communications of the ACM* 64.9 (2021), pp. 99–106.
- 645 [46] Frank Seide et al. “1-bit stochastic gradient descent and its application to data-parallel
 646 distributed training of speech dnns”. In: *Fifteenth annual conference of the international
 647 speech communication association*. 2014.

- 648 [47] Noam Shazeer and Mitchell Stern. “Adafactor: Adaptive learning rates with sublin-
 649 ear memory cost”. In: *International Conference on Machine Learning*. PMLR. 2018,
 650 pp. 4596–4604.
- 651 [48] Mohammad Shoeybi et al. “Megatron-lm: Training multi-billion parameter language
 652 models using model parallelism”. In: *arXiv preprint arXiv:1909.08053* (2019).
- 653 [49] Hanlin Tang et al. “1-bit adam: Communication efficient large-scale training with
 654 adam’s convergence speed”. In: *International Conference on Machine Learning*. PMLR.
 655 2021, pp. 10118–10129.
- 656 [50] Yuandong Tian et al. “Joma: Demystifying multilayer transformers via joint dynamics
 657 of mlp and attention”. In: *arXiv preprint arXiv:2310.00535* (2023).
- 658 [51] Hugo Touvron et al. “Llama 2: Open foundation and fine-tuned chat models”. In: *arXiv
 659 preprint arXiv:2307.09288* (2023).
- 660 [52] Hugo Touvron et al. “Llama: Open and efficient foundation language models”. In: *arXiv
 661 preprint arXiv:2302.13971* (2023).
- 662 [53] Alexander Tyurin and Peter Richtárik. “DASHA: Distributed nonconvex optimization
 663 with communication compression, optimal oracle complexity, and no client synchroniza-
 664 tion”. In: *arXiv preprint arXiv:2202.01268* (2022).
- 665 [54] Ashish Vaswani et al. “Attention is all you need”. In: *Advances in neural information
 666 processing systems* 30 (2017).
- 667 [55] Thijs Vogels, Sai Praneeth Karimireddy, and Martin Jaggi. “PowerSGD: Practical
 668 low-rank gradient compression for distributed optimization”. In: *Advances in Neural
 669 Information Processing Systems* 32 (2019).
- 670 [56] Guanhua Wang et al. “Zero++: Extremely efficient collective communication for giant
 671 model training”. In: *arXiv preprint arXiv:2306.10209* (2023).
- 672 [57] Hongyi Wang et al. “Atomo: Communication-efficient learning via atomic sparsification”.
 673 In: *Advances in neural information processing systems* 31 (2018).
- 674 [58] Wenhan Xia, Chengwei Qin, and Elad Hazan. “Chain of lora: Efficient fine-tuning of
 675 language models via residual learning”. In: *arXiv preprint arXiv:2401.04151* (2024).
- 676 [59] Hang Xu et al. “Compressed communication for distributed deep learning: Survey and
 677 quantitative evaluation”. In: (2020).
- 678 [60] Greg Yang, James B Simon, and Jeremy Bernstein. “A spectral condition for feature
 679 learning”. In: *arXiv preprint arXiv:2310.17813* (2023).
- 680 [61] Pengyun Yue et al. *CORE: Common Random Reconstruction for Distributed Opti-
 681 mization with Provable Low Communication Complexity*. 2023. arXiv: 2309 . 13307
 682 [cs.LG].
- 683 [62] Rowan Zellers et al. “Hellaswag: Can a machine really finish your sentence?” In: *arXiv
 684 preprint arXiv:1905.07830* (2019).
- 685 [63] Renrui Zhang et al. “Llama-adapter: Efficient fine-tuning of language models with
 686 zero-init attention”. In: *arXiv preprint arXiv:2303.16199* (2023).
- 687 [64] Jiawei Zhao et al. “Galore: Memory-efficient llm training by gradient low-rank projec-
 688 tion”. In: *arXiv preprint arXiv:2403.03507* (2024).
- 689 [65] Yanli Zhao et al. “Pytorch fsdp: experiences on scaling fully sharded data parallel”. In:
 690 *arXiv preprint arXiv:2304.11277* (2023).
- 691
 692
 693
 694
 695
 696
 697
 698
 699
 700
 701

702 **Algorithm 2** SEPARATE: PyTorch-like

```

703     random_variable_buffer.Initialization() # initialize the variable buffer
704     def Communication_hook (model.weight): # definition hook function for overlap
705         computation
706         projected_grad = Project (grad, random_variable_buffer) # random project the
707         grad
708         Communication(projected_grad)
709         grad = Reproject(projected_grad, random_variable_buffer )
710         random_variable_buffer.Update() # update variable buffer with new random variables
711         for model.weight in model.weights:
712             model.weight.register_hook(Communication_hook)
713             # register hook for each layer's weight of the model

```

714
715 **A DISCUSSION**

716 In this section, we make a discussion about some related methods for memory-efficient
 717 training, the details of our method application, and the robustness. Such a discussion
 718 provides us with a clearer understanding of the domain, practicability, and extensibility of
 719 our method.

720 **Compared with Memory-Efficient Training.** Memory-efficient training is another
 721 area of efficient training, focusing on how to reduce the memory cost during training
 722 process. We notice that random projection is also used for memory reduction, such as
 723 Flora for gradient accumulation [19] and GaLore for memory-efficient update in compact
 724 space [64]. These approaches seem to show similarity and potential in combination with
 725 our method, but we consider different sides of efficient training. It is usually a trade-off
 726 because there are key bottlenecks about the extra computational cost for memory reduction.
 727 Communication in modern LLMs training framework (e.g., Megatron-LM [48]) overlaps
 728 between local computation and global all-reduce. This allows us to tolerate only minimal
 729 extra computational preprocessing overhead, lest long synchronization times cause the wall-
 730 clock training time to rise. One matrix projection is almost at the limit of tolerance, and
 731 SVD is almost intolerable. To the best of our knowledge, only our "simple but efficient
 732 operation" can manage to reduce the training wall-clock time.

733 **Details of SEPARATE Application.** For the common random projection compressor
 734 shown in Algorithm 1, we introduce common random vector generators on different nodes of
 735 the distributed training clusters. This setup leads our analysis, but it does not incur any
 736 additional overhead in actual application, because we can easily set a dedicated common
 737 random seed to generate the same random variables on each node during initialization.
 738 Moreover, we could easily apply SEPARATE to all kinds of gradient-based optimizers and
 739 can be regarded as a plug-in, which can be simply implemented with a few lines of code in
 740 off-the-shelf frameworks as shown in Algorithm 2. This means that our method is also the
 741 first gradient compression technique that can be seamlessly integrated with FSDP rather
 742 than DDP to the best of our knowledge.

743 **Robustness with Few Parameter Tuning.** We expect to propose a simple and effective
 744 gradient compression method that can be efficiently adapted to existing LLMs training
 745 frameworks. Therefore, we expect the method to have a certain degree of robustness,
 746 that is, it does not depend on the resetting of hyperparameters. In our experiments, all
 747 hyperparameters are derived from the default settings of the corresponding model trained
 748 under the corresponding framework. In other words, we do not adjust the hyperparameters
 749 individually for SEPARATE. We show the hyperparameters setting in Appendix E. In
 750 addition, the method introduces the compression ratio. Our variance analysis and the
 751 main theorem demonstrate that, provided the selection of the compression ratio aligns with
 752 the conditions in our theoretical analysis (Theorem 5.5 and 5.7), our method can exhibit
 753 effective performance. This theoretical underpinning ensures that our method is robust
 754 within the specified compression ratio. Second, in practical applications, especially for models
 755 with a substantial number of parameters, such as those in the millions or billions, we can

756 defaultly set the compression ratio as 16, 32 or 64. As illustrated in Table 3, the performance
 757 differences between compression ratios of 16, 32, or 64 times for gradient information are
 758 minimal. Consequently, the choice of compression ratio is more influenced by the user's
 759 device constraints rather than the intrinsic characteristics of the model.
 760

761 B PROPERTIES OF SEPARATE COMPRESSOR 762

763 In this section, we propose several properties of the expectation and variance of the common
 764 random projection compressor in SEPARATE. The first analysis of such properties is
 765 proposed in the research of distributed optimization theory [61]. Let \mathbf{a} represent the vector
 766 for communication and $\tilde{\mathbf{a}}$ represent the estimate one generated by the compressor. In Lemma
 767 4.1 and Lemma 4.2, we show that $\tilde{\mathbf{a}}$ is an unbiased estimator, and the variance of $\tilde{\mathbf{a}}$ can be
 768 $\text{tr}(\mathbf{A})$ -bounded under arbitrary matrix \mathbf{A} -norms, respectively.

769 **Lemma B.1.** $\tilde{\mathbf{a}}$ is an unbiased estimator of \mathbf{a} ,

$$770 \quad \mathbb{E}_{\xi_1, \dots, \xi_m} \tilde{\mathbf{a}} = \mathbf{a}. \quad (14)$$

772 *Proof of Lemma 4.1.*

$$\begin{aligned} 773 \quad \mathbb{E}_{\xi_1, \dots, \xi_m} \tilde{\mathbf{a}} &= \mathbb{E}_{\xi_1, \dots, \xi_m} \left[\frac{1}{m} \sum_{i=1}^m \langle \mathbf{a}, \xi_i \rangle \cdot \xi_i \right] \\ 774 &= \mathbb{E}_{\xi_1} \xi_1 \xi_1^\top \mathbf{a} = \mathbf{I}\mathbf{a} \\ 775 &= \mathbf{a} \end{aligned} \quad (15)$$

776 \square

777 **Lemma B.2.** The variance of $\tilde{\mathbf{a}}$ under norm $\|\cdot\|_{\mathbf{A}}$, where \mathbf{A} is a given positive semi-definite
 778 symmetric matrix, can be bounded by $\frac{3\text{tr}(\mathbf{A})}{m} \|\mathbf{a}\|^2 - \frac{1}{m} \|\mathbf{a}\|_{\mathbf{A}}^2$,

$$779 \quad \mathbb{E}_{\xi_1, \dots, \xi_m} \|\tilde{\mathbf{a}} - \mathbf{a}\|_{\mathbf{A}}^2 \leq \frac{3\text{tr}(\mathbf{A})}{m} \|\mathbf{a}\|^2 - \frac{1}{m} \|\mathbf{a}\|_{\mathbf{A}}^2. \quad (16)$$

780 *Proof of Lemma 4.2.* For the simplicity of notation, we use \mathbb{E}_{ξ} to denote $\mathbb{E}_{\xi_1, \dots, \xi_m}$.

$$\begin{aligned} 781 \quad \mathbb{E}_{\xi} \|\tilde{\mathbf{a}} - \mathbf{a}\|_{\mathbf{A}}^2 &= \mathbb{E}_{\xi} \left\| \frac{1}{m} \sum_{i=1}^m (\langle \mathbf{a}, \xi_i \rangle \cdot \xi_i - \mathbf{a}) \right\|_{\mathbf{A}}^2 \\ 782 &= \mathbb{E}_{\xi} \left[\frac{1}{m^2} \sum_{i=1}^m (\mathbf{a}^\top \xi_i \xi_i^\top \mathbf{A} \xi_i \xi_i^\top \mathbf{a} - \mathbf{a}^\top \mathbf{A} \mathbf{a}) \right] \\ 783 &= \frac{1}{m} \mathbb{E}_{\xi_1} \mathbf{a}^\top \xi_1 \xi_1^\top \mathbf{A} \xi_1 \xi_1^\top \mathbf{a} - \frac{1}{m} \|\mathbf{a}\|_{\mathbf{A}}^2. \end{aligned} \quad (17)$$

784 Let $\mathbf{A} = \mathbf{U}^\top \mathbf{D} \mathbf{U}$ be the eigenvalue decomposition of \mathbf{A} where $\mathbf{D} = \text{diag}\{b_1, \dots, b_d\}$ is a
 785 diagonal matrix, and $\zeta = \mathbf{U} \xi_1$ be a linear transformation of the random variable ξ_1 . We
 786 have

$$\begin{aligned} 787 \quad \mathbb{E}_{\xi_1} [\xi_1 \xi_1^\top \mathbf{A} \xi_1 \xi_1^\top] &\stackrel{a}{=} \mathbb{E}_{\zeta} [\mathbf{U}^\top \zeta \zeta^\top \mathbf{D} \zeta \zeta^\top \mathbf{U}] \\ 788 &= \mathbf{U}^\top \mathbb{E}_{\zeta} \left[\sum_{i=1}^d b_i \zeta_i^2 \cdot \zeta \zeta^\top \right] \mathbf{U} \\ 789 &\stackrel{b}{=} \mathbf{U}^\top \left(\sum_{i=1}^d b_i \cdot \mathbf{I} + 2\mathbf{D} \right) \mathbf{U} \\ 790 &\stackrel{c}{=} \text{tr}(\mathbf{A}) \cdot \mathbf{I} + 2\mathbf{A} \\ 791 &\preceq 3\text{tr}(\mathbf{A}) \cdot \mathbf{I}. \end{aligned} \quad (18)$$

792 In $\stackrel{a}{=}$, we use $\zeta \sim N(0, \mathbf{I}_d)$ based on the rotational invariance of the standard Gaussian
 793 distribution. In $\stackrel{b}{=}$, we use the second and forth moment of standard Gaussian variables:

810 $\mathbb{E}\zeta_i^2 = 1$ and $\mathbb{E}\zeta_i^4 = 3$. In $\stackrel{c}{=}$, we use $\text{tr}(\mathbf{U}^\top \mathbf{D}\mathbf{U}) = \text{tr}(\mathbf{U}^\top \mathbf{U}\mathbf{D}) = \text{tr}(\mathbf{D})$. The last inequality
 811 of (18) is due to $\text{tr}(\mathbf{A}) \cdot \mathbf{I} \succeq \mathbf{A}$. Combining (18) and (17), we have

$$813 \quad \mathbb{E}_{\xi_1, \dots, \xi_m} \|\tilde{\mathbf{a}} - \mathbf{a}\|_{\mathbf{A}}^2 \leq \frac{3\text{tr}(\mathbf{A})}{m} \|\mathbf{a}\|^2 - \frac{1}{m} \|\mathbf{a}\|_{\mathbf{A}}^2. \quad (19)$$

815 \square

816

817 C DEFERRED PROOF IN SECTION 5
818819 C.1 USEFUL LEMMAS
820

821 In this Section, we propose several useful lemmas for the proof of our main theorem in
822 Section 5.

823 **Lemma C.1.** *For the gradient $\tilde{\mathbf{h}}_n^k = \frac{1}{m} \sum_{i=1}^m \tilde{p}_i \cdot \xi_i$ where $\tilde{p}_i = \frac{1}{N} \sum_{n=1}^N p_{i,n}$ is the global
824 average of $p_{i,n}$ in each machine after communication in Algorithm 1, we have*

$$825 \quad \tilde{\mathbf{h}}^k = \mathbf{g}^k + \frac{1}{\beta} (\mathbf{e}^k - \mathbf{e}^{k+1}), \quad (20)$$

826 where $\tilde{\mathbf{h}}^k = \frac{1}{N} \sum_{n=1}^N \tilde{\mathbf{h}}_n^k$, $\mathbf{g}^k = \frac{1}{N} \sum_{n=1}^N \mathbf{g}_n^k$ and $\mathbf{e}^k = \frac{1}{N} \sum_{n=1}^N \mathbf{e}_n^k$.

827 *Proof of Lemma C.1.* For the estimate $\tilde{\mathbf{h}}^k$ defined in Lemma C.1, we have

$$\begin{aligned} 828 \quad \tilde{\mathbf{h}}^k &= \frac{1}{N} \sum_{n=1}^N \tilde{\mathbf{h}}_n^k \\ 829 &= \frac{1}{N} \sum_{n=1}^N \frac{1}{m} \sum_{i=1}^m \frac{1}{N} \sum_{n=1}^N \langle \mathbf{h}_n^k, \xi_i \rangle \cdot \xi_i \\ 830 &= \frac{1}{m} \sum_{i=1}^m \frac{1}{N} \sum_{n=1}^N \langle \mathbf{h}_n^k, \xi_i \rangle \cdot \xi_i \\ 831 &= \frac{1}{N} \sum_{n=1}^N \left(\mathbf{h}_n^k + \frac{1}{m} \sum_{i=1}^m \langle \mathbf{h}_n^k, \xi_i \rangle \cdot \xi_i - \mathbf{h}_n^k \right) \\ 832 &= \frac{1}{N} \sum_{n=1}^N \mathbf{g}_n^k + \mathbf{e}_n^k - \delta_n^k \end{aligned} \quad (21)$$

833 where $\delta_n^k = \mathbf{h}_n^k - \frac{1}{m} \sum_{i=1}^m \langle \mathbf{h}_n^k, \xi_i \rangle \cdot \xi_i$. Taking average of δ_n^k , we have

$$\begin{aligned} 834 \quad \delta^k &= \frac{1}{N} \sum_{n=1}^N \left(\mathbf{h}_n^k - \frac{1}{m} \sum_{i=1}^m \langle \mathbf{h}_n^k, \xi_i \rangle \cdot \xi_i \right) \\ 835 &= \mathbf{h}^k - \tilde{\mathbf{h}}^k \\ 836 &= \frac{1}{\beta} (\mathbf{e}^{k+1} - (1-\beta)\mathbf{e}^k), \end{aligned} \quad (22)$$

837 where the last equality uses $\mathbf{e}^{k+1} = (1-\beta)\mathbf{e}^k + \beta(\mathbf{h}^k - \tilde{\mathbf{h}}^k)$ which is the average of the
838 iteration of \mathbf{e}_n^{k+1} in Algorithm 1. Combining the two equalities above, we have

$$839 \quad \tilde{\mathbf{h}}^k = \mathbf{g}^k + \mathbf{e}^k - \delta^k = \mathbf{g}^k + \frac{1}{\beta} (\mathbf{e}^k - \mathbf{e}^{k+1}). \quad (23)$$

840

841 We complete the proof of Lemma C.1. \square

842 **Lemma C.2.** *Suppose the setting in Theorem 5.5 hold, and we use $\tilde{\mathbf{h}}^k$ in Algorithm 1 to
843 update the model weight θ^k in SGD as*

$$844 \quad \theta^{k+1} = \theta^k - \eta \tilde{\mathbf{h}}^k. \quad (24)$$

864 Then we have

$$\mathbb{E} \left\| \sum_{i=0}^k (\tilde{\mathbf{h}}^i - \mathbf{g}^i) \right\| \leq \frac{1 + (1-\beta)^{k+1}}{\beta} c_1. \quad (25)$$

869 Proof of Lemma C.2. Consider the expectation of $\|\mathbf{e}^{k+1}\|$ about the random Gaussian vari-
870 ables ξ_1, \dots, ξ_m and the stochastic mini-batch as below

$$871 \mathbb{E} \|\mathbf{e}^{k+1}\| = \mathbb{E} [\mathbb{E}_{\xi_1, \dots, \xi_m} \|\mathbf{e}^{k+1}\|]. \quad (26)$$

872 First we have

$$\begin{aligned} 873 \mathbb{E}_{\xi_1, \dots, \xi_m} \|\mathbf{e}^{k+1}\| &= \mathbb{E}_{\xi_1, \dots, \xi_m} \|(1-\beta)\mathbf{e}^k + \beta(\mathbf{h}^k - \tilde{\mathbf{h}}^k)\| \\ 874 &\leq (1-\beta)\mathbb{E}_{\xi_1, \dots, \xi_m} \|\mathbf{e}^k\| + \mathbb{E}_{\xi_1, \dots, \xi_m} \|\beta(\mathbf{h}^k - \tilde{\mathbf{h}}^k)\| \\ 875 &= (1-\beta)\|\mathbf{e}^k\|, \\ 876 \end{aligned} \quad (27)$$

877 where the first inequality uses $\tilde{\mathbf{h}}^k$ is the unbiased estimate of \mathbf{h}^k . Thus we have

$$878 \mathbb{E} \|\mathbf{e}^{k+1}\| \leq (1-\beta)\mathbb{E} \|\mathbf{e}^k\| \leq (1-\beta)^{k+1} \|\mathbf{e}^0\| \leq (1-\beta)^{k+1} c_1. \quad (28)$$

880 Considering the accumulated bias of $\tilde{\mathbf{h}}^k$ and \mathbf{h}^k , based on Lemma C.1 we have

$$\begin{aligned} 881 \mathbb{E} \left\| \sum_{i=0}^k (\tilde{\mathbf{h}}^i - \mathbf{g}^i) \right\| &= \frac{1}{\beta} \mathbb{E} \left\| \sum_{i=0}^k \mathbf{e}^i - \mathbf{e}^{i+1} \right\| \leq \frac{1}{\beta} (\mathbb{E} \|\mathbf{e}^{k+1}\| + c_1) \leq \frac{1 + (1-\beta)^{k+1}}{\beta} c_1. \\ 882 \\ 883 \end{aligned} \quad (29)$$

□

885 **Lemma C.3.** Suppose the setting in Theorem 5.7 hold, and we use $\tilde{\mathbf{h}}^k$ in Algorithm 1 to
886 update te model weight θ^k in Adam-Type optimizers as (8). Then consider the following two
887 sequences $\{\mathbf{m}^k\}_{k=0}^K$ and $\{\tilde{\mathbf{m}}^k\}_{k=0}^K$ as:

$$\begin{aligned} 888 \mathbf{m}^k &= (1-\beta_1)\mathbf{m}^{k-1} + \beta_1 \mathbf{g}^k, \\ 889 \tilde{\mathbf{m}}^k &= (1-\beta_1)\tilde{\mathbf{m}}^{k-1} + \beta_1 \tilde{\mathbf{h}}^k. \end{aligned} \quad (30)$$

891 Assume that for the sequence $\{\eta^k\}_{k=0}^K$, each element of η^k satisfies

$$893 \eta c_l \leq \eta_i^k \leq \eta c_u, \quad |\eta_i^k - \eta_i^{k-1}| \leq \eta \beta_1 (1-\beta_1)^{K-k} c_u, \forall i \in [d], k \in [K]. \quad (31)$$

894 Then we have

$$895 \mathbb{E} \left\| \sum_{i=0}^K \boldsymbol{\eta}^i \circ (\tilde{\mathbf{m}}^i - \mathbf{m}^i) \right\| \leq \frac{2c_1 c_u \eta \sqrt{d}}{\beta}. \quad (32)$$

898 Proof of Lemma C.3. First we extend the iterations of $\{\mathbf{m}^k\}_{k=0}^K$ and $\{\tilde{\mathbf{m}}^k\}_{k=0}^K$:

$$900 \mathbf{m}^k = (1-\beta_1)\mathbf{m}^{k-1} + \beta_1 \mathbf{g}^k = (1-\beta_1)^{k-1} \mathbf{m}^0 + \beta_1 \sum_{t=1}^k (1-\beta_1)^{k-t} \mathbf{g}^t, \quad (33)$$

902 and

$$904 \tilde{\mathbf{m}}^k = (1-\beta_1)\tilde{\mathbf{m}}^{k-1} + \beta_1 \tilde{\mathbf{h}}^k = (1-\beta_1)^{k-1} \mathbf{m}^0 + \beta_1 \sum_{t=1}^k (1-\beta_1)^{k-t} \tilde{\mathbf{h}}^t. \quad (34)$$

906 Based on Lemma C.1, we have

$$908 \sum_{i=0}^k \boldsymbol{\eta}^i \circ (\tilde{\mathbf{m}}^i - \mathbf{m}^i) \leq \frac{\beta_1}{\beta} \sum_{i=0}^k \boldsymbol{\eta}^i \circ \left(\sum_{t=0}^i (1-\beta_1)^{i-t} (\mathbf{e}^t - \mathbf{e}^{t+1}) \right). \quad (35)$$

910 Then we element-wisely analyse the upper bound of the accumulated error as below. We
911 use the non-blackbody letters to represent the element of vectors for convenience with some
912 symbolic abuse.

$$\begin{aligned} 914 &\left| \frac{\beta_1}{\beta} \sum_{i=0}^k \eta^i \sum_{t=0}^i (1-\beta_1)^{i-t} (e^t - e^{t+1}) \right| \\ 915 \\ 916 &= \left| \frac{\beta_1}{\beta} \sum_{t=0}^k \left(\sum_{i=t}^{k-1} (\eta^i - \eta^{i-1})(1-\beta_1)^{i-t} - \eta^{k-1}(1-\beta_1)^{k-t} \right) e^t \right|. \end{aligned} \quad (36)$$

918 Then using Lemma C.2, we take the expectation of the accumulated error as below:
919

$$\begin{aligned}
& \mathbb{E} \left\| \sum_{i=0}^k \boldsymbol{\eta}^i \circ (\tilde{\mathbf{m}}^i - \mathbf{m}^i) \right\| \\
& \leq \sqrt{d} \cdot \mathbb{E} \left\| \sum_{i=0}^k \boldsymbol{\eta}^i \circ (\tilde{\mathbf{m}}^i - \mathbf{m}^i) \right\|_\infty \\
& \leq \sqrt{d} \cdot \mathbb{E} \sup_{n \in [d]} \left| \frac{\beta_1}{\beta} \sum_{t=0}^k \left(\sum_{i=t}^{k-1} (\eta_n^i - \eta_n^{i-1})(1 - \beta_1)^{i-t} - \eta_n^{k-1}(1 - \beta_1)^{k-t} \right) e_n^t \right| \quad (37) \\
& \leq \frac{\beta_1 c_1 c_u \eta \sqrt{d}}{\beta} \mathbb{E} \left| \beta_1 \sum_{t=1}^{k-1} t(1 - \beta_1)^t + \sum_{t=1}^{k-1} (1 - \beta_1)^t \right| \\
& \leq \frac{2c_1 c_u \eta \sqrt{d}}{\beta}.
\end{aligned}$$

934 For the first inequality we use the property of vector norm that $\|\cdot\| \leq \sqrt{d}\|\cdot\|_\infty$. For the
935 second inequality we use the definition of vector's infinite norm. For the third inequality
936 we use the assumption that $|\eta^i - \eta^{i-1}| \leq \eta \beta_1 (1 - \beta_1)^{K-i} c_u, \forall i \in [K]$ to obtain the upper
937 bound of each element, and use Lemma C.2 to estimate the upper bound of $\mathbb{E}|e_n^t|$ that
938 $\mathbb{E}|e_n^t| \leq \mathbb{E}|e_n^0| \leq c_1$. For the forth inequality we use the summation of series to obtain that
939 $\beta_1 \sum_{t=1}^{k-1} t(1 - \beta_1)^t + \sum_{t=1}^{k-1} (1 - \beta_1)^t \leq \frac{2}{\beta_1}$. Thus we have

$$\mathbb{E} \left\| \sum_{i=0}^k \boldsymbol{\eta}^i \circ (\tilde{\mathbf{m}}^i - \mathbf{m}^i) \right\| \leq \frac{2c_1 c_u \eta \sqrt{d}}{\beta}. \quad (38)$$

□

940
941
942
943
944 **Lemma C.4.** Consider the moving average iteration like AdamType as

$$\mathbf{m}^k = (1 - \beta)\mathbf{m}^{k-1} + \beta \mathbf{g}^k, \quad (39)$$

945 where $\mathbf{g}^k = \nabla f(\boldsymbol{\theta}^k) + \boldsymbol{\xi}^k$ is the stochastic gradient with $\mathbb{E}\boldsymbol{\xi}^k = 0$ and $\mathbb{E}\|\boldsymbol{\xi}^k\|^2 \leq \sigma^2$. Then we
946 have

$$\mathbb{E} \|\mathbf{m}^k - \nabla f(\boldsymbol{\theta}^k)\|^2 \leq (1 - \beta) \mathbb{E} \|\mathbf{m}^{k-1} - \nabla f(\boldsymbol{\theta}^{k-1})\|^2 + \frac{(1 - \beta)^2 L^2}{\beta} \mathbb{E} \|\boldsymbol{\theta}^{k-1} - \boldsymbol{\theta}^k\|^2 + \beta^2 \sigma^2. \quad (40)$$

947
948 *Proof of Lemma C.4.* Based on the iteration of \mathbf{m} we have

$$\mathbf{m}^k - \nabla f(\boldsymbol{\theta}^k) = (1 - \beta)(\mathbf{m}^{k-1} - \nabla f(\boldsymbol{\theta}^{k-1})) + (1 - \beta)(\nabla f(\boldsymbol{\theta}^{k-1}) - \nabla f(\boldsymbol{\theta}^k)) + \beta(\mathbf{g}^k - \nabla f(\boldsymbol{\theta}^k)). \quad (41)$$

949 Then taking expectation of both sides we have

$$\begin{aligned}
\mathbb{E} \|\mathbf{m}^k - \nabla f(\boldsymbol{\theta}^k)\|^2 &= (1 - \beta)^2 \mathbb{E} \|\mathbf{m}^{k-1} - \nabla f(\boldsymbol{\theta}^{k-1})\|^2 + (1 - \beta)^2 \mathbb{E} \|\nabla f(\boldsymbol{\theta}^{k-1}) - \nabla f(\boldsymbol{\theta}^{k-1})\|^2 \\
&\quad + \beta^2 \sigma^2 + 2(1 - \beta)^2 \mathbb{E} \langle \mathbf{m}^{k-1} - \nabla f(\boldsymbol{\theta}^{k-1}), \nabla f(\boldsymbol{\theta}^{k-1}) - \nabla f(\boldsymbol{\theta}^{k-1}) \rangle \\
&\leq (1 - \beta)^2 (1 + a) \mathbb{E} \|\mathbf{m}^{k-1} - \nabla f(\boldsymbol{\theta}^{k-1})\|^2 \\
&\quad + (1 - \beta)^2 \left(1 + \frac{1}{a} \right) \mathbb{E} \|\nabla f(\boldsymbol{\theta}^{k-1}) - \nabla f(\boldsymbol{\theta}^{k-1})\|^2 + \beta^2 \sigma^2 \\
&\leq (1 - \beta) \mathbb{E} \|\mathbf{m}^{k-1} - \nabla f(\boldsymbol{\theta}^{k-1})\|^2 \\
&\quad + \frac{(1 - \beta)^2}{\beta} \mathbb{E} \|\nabla f(\boldsymbol{\theta}^{k-1}) - \nabla f(\boldsymbol{\theta}^{k-1})\|^2 + \beta^2 \sigma^2 \\
&\leq (1 - \beta) \mathbb{E} \|\mathbf{m}^{k-1} - \nabla f(\boldsymbol{\theta}^{k-1})\|^2 + \frac{(1 - \beta)^2 L^2}{\beta} \mathbb{E} \|\boldsymbol{\theta}^{k-1} - \boldsymbol{\theta}^k\|^2 + \beta^2 \sigma^2.
\end{aligned} \quad (42)$$

□

972 C.2 PROOF OF THEOREM 5.5
 973

974 *Proof.* Consider the two SGD-based iteration $\{\boldsymbol{\theta}^k\}_{k=1}^K$ as:

$$976 \quad \boldsymbol{\theta}^{k+1} = \boldsymbol{\theta}^k - \eta \mathbf{g}^k = \boldsymbol{\theta}^0 - \eta \sum_{i=0}^k \mathbf{g}^i \quad (43)$$

979 and $\{\tilde{\boldsymbol{\theta}}^k\}_{k=1}^K$ as:

$$981 \quad \tilde{\boldsymbol{\theta}}^{k+1} = \tilde{\boldsymbol{\theta}}^k - \eta \tilde{\mathbf{h}}^k = \boldsymbol{\theta}^0 - \eta \sum_{i=0}^k \mathbf{g}^i + \eta \sum_{i=0}^k (\mathbf{g}^i - \tilde{\mathbf{h}}^i). \quad (44)$$

984 For $k \in [K]$, due to the L -smooth assumption of the objective f and Lemma C.1, we have

$$987 \quad \mathbb{E} \left\| \nabla f(\tilde{\boldsymbol{\theta}}^k) - \nabla f(\boldsymbol{\theta}^k) \right\| \leq L \mathbb{E} \left\| \tilde{\boldsymbol{\theta}}^k - \boldsymbol{\theta}^k \right\| = \eta L \mathbb{E} \left\| \sum_{i=0}^{k-1} (\mathbf{g}^i - \tilde{\mathbf{h}}^i) \right\| \leq \frac{(1 + (1 - \beta)^k) \eta L c_1}{\beta}. \quad (45)$$

990 Next, we write the second-order Taylor expansion of $f(\boldsymbol{\theta}^{k+1})$ at $\boldsymbol{\theta}^k$ as below:

$$992 \quad f(\boldsymbol{\theta}^{k+1}) \leq f(\boldsymbol{\theta}^k) + \langle \nabla f(\boldsymbol{\theta}^k), \boldsymbol{\theta}^{k+1} - \boldsymbol{\theta}^k \rangle + \frac{1}{2} \langle \mathbf{A}(\boldsymbol{\theta}^{k+1} - \boldsymbol{\theta}^k), \boldsymbol{\theta}^{k+1} - \boldsymbol{\theta}^k \rangle. \quad (46)$$

995 Taking expectation of (46) with condition on the iteration before k and random Gaussian
 996 variables to both sides of (46), using Lemma 4.1, Lemma 4.2 and Assumption 5.4, we have

$$997 \quad \begin{aligned} \mathbb{E} f(\boldsymbol{\theta}^{k+1}) &\leq \mathbb{E} \left[f(\boldsymbol{\theta}^k) + \langle \nabla f(\boldsymbol{\theta}^k), \boldsymbol{\theta}^{k+1} - \boldsymbol{\theta}^k \rangle + \eta^2 \left(\frac{3 \text{tr}(\nabla^2 f(\boldsymbol{\theta}^k))}{2m} \left\| \nabla f(\tilde{\boldsymbol{\theta}}^k) \right\|^2 + \left\| \nabla f(\tilde{\boldsymbol{\theta}}^k) \right\|_{\mathbf{A}}^2 \right) \right] \\ 1000 &\leq \mathbb{E} f(\boldsymbol{\theta}^k) - \eta \mathbb{E} \langle \nabla f(\boldsymbol{\theta}^k), \nabla f(\tilde{\boldsymbol{\theta}}^k) \rangle + \eta \mathbb{E} \langle \nabla f(\boldsymbol{\theta}^k), \nabla f(\tilde{\boldsymbol{\theta}}^k) - \nabla f(\boldsymbol{\theta}^k) \rangle \\ 1001 &\quad + \eta^2 \left(\frac{3 \text{tr}(\mathbf{A})}{2m} + L \right) \mathbb{E} \left\| \nabla f(\tilde{\boldsymbol{\theta}}^k) \right\|^2 \\ 1004 &\stackrel{a}{\leq} \mathbb{E} f(\boldsymbol{\theta}^k) - \eta \left\| \nabla f(\tilde{\boldsymbol{\theta}}^k) \right\|^2 + \eta \mathbb{E} \langle \nabla f(\boldsymbol{\theta}^k), \nabla f(\tilde{\boldsymbol{\theta}}^k) - \nabla f(\boldsymbol{\theta}^k) \rangle \\ 1005 &\quad + \eta \mathbb{E} \langle \nabla f(\tilde{\boldsymbol{\theta}}^k) - \nabla f(\boldsymbol{\theta}^k), \nabla f(\tilde{\boldsymbol{\theta}}^k) \rangle + \eta^2 \cdot \frac{5 \text{tr}(\mathbf{A})}{2m} \mathbb{E} \left\| \nabla f(\tilde{\boldsymbol{\theta}}^k) \right\|^2 \\ 1008 &\leq \mathbb{E} f(\boldsymbol{\theta}^k) - \eta \left\| \nabla f(\tilde{\boldsymbol{\theta}}^k) \right\|^2 + \mathcal{O} \left(\eta \left(\frac{(1 + (1 - \beta)^k) \eta L c_1}{\beta} \sqrt{d c_\infty} \right) \right) \\ 1011 &\quad + \eta^2 \cdot \frac{5 \text{tr}(\mathbf{A})}{2m} \left(\left\| \nabla f(\tilde{\boldsymbol{\theta}}^k) \right\|^2 + \frac{\sigma^2}{N} \right) \end{aligned} \quad (47)$$

1014 where in $\stackrel{a}{\leq}$ we use $m \leq \frac{\text{tr}(\mathbf{A})}{L}$. Then, using $\eta \leq \frac{m}{4 \text{tr}(\mathbf{A})}$, we have

$$1017 \quad \frac{1}{K} \sum_{k=0}^K \mathbb{E} \left\| \nabla f(\tilde{\boldsymbol{\theta}}^k) \right\|^2 \leq \frac{8 \left(f(\tilde{\boldsymbol{\theta}}^0) - f(\tilde{\boldsymbol{\theta}}^*) \right)}{3\eta K} + \mathcal{O} \left(\frac{(2 - \beta) \eta L c_1}{\beta} \sqrt{d c_\infty} \right) + \mathcal{O} \left(\frac{\eta \sigma^2}{N} \right). \quad (48)$$

1020 By letting $\eta = \mathcal{O}(d^{-1/2} \epsilon^2)$, $K = \Omega(d^{1/2} \epsilon^{-4})$. we have

$$1023 \quad \frac{1}{K} \sum_{k=0}^K \mathbb{E} \left\| \nabla f(\tilde{\boldsymbol{\theta}}^k) \right\|^2 \leq \mathcal{O} \left(\epsilon^2 \left(f(\tilde{\boldsymbol{\theta}}^0) - f(\tilde{\boldsymbol{\theta}}^*) + \frac{(2 - \beta) L c_1}{\beta} c_\infty + \frac{\sigma^2}{N} \right) \right) = \mathcal{O}(\epsilon^2). \quad (49)$$

1025 Thus we finish the proof of Theorem 5.5. \square

1026 C.3 PROOF OF THEOREM 5.7
 1027

1028 *Proof.* We also consider two AdamType-based iteration $\{\boldsymbol{\theta}^k\}_{k=1}^K$ as:

$$1029 \quad \boldsymbol{\theta}^{k+1} = \boldsymbol{\theta}^k - \boldsymbol{\eta}^k \circ \mathbf{m}^k = \boldsymbol{\theta}^0 - \sum_{i=0}^k \boldsymbol{\eta}^i \circ \mathbf{m}^i, \quad (50)$$

1030 where $\mathbf{m}^k = (1 - \beta_1)\mathbf{m}^{k-1} + \beta_1 \mathbf{g}^k$, and $\{\tilde{\boldsymbol{\theta}}^k\}_{k=1}^K$ as:

$$1031 \quad \tilde{\boldsymbol{\theta}}^{k+1} = \tilde{\boldsymbol{\theta}}^k - \boldsymbol{\eta}^k \circ \tilde{\mathbf{m}}^k = \boldsymbol{\theta}^0 - \sum_{i=0}^k \boldsymbol{\eta}^i \circ \tilde{\mathbf{m}}^i = \boldsymbol{\theta}^0 - \sum_{i=0}^k \boldsymbol{\eta}^i \circ \mathbf{m}^i + \sum_{i=0}^k \boldsymbol{\eta}^i \circ (\mathbf{m}^i - \tilde{\mathbf{m}}^i), \quad (51)$$

1032 where $\tilde{\mathbf{m}}^k = (1 - \beta_1)\tilde{\mathbf{m}}^{k-1} + \beta_1 \mathbf{h}^k$. Based on Lemma C.3, we have

$$1033 \quad \mathbb{E} \left\| \nabla f(\tilde{\boldsymbol{\theta}}^k) - \nabla f(\boldsymbol{\theta}^k) \right\| \leq L \mathbb{E} \left\| \tilde{\boldsymbol{\theta}}^k - \boldsymbol{\theta}^k \right\| = L \mathbb{E} \left\| \sum_{i=0}^k \boldsymbol{\eta}^i \circ (\mathbf{m}^i - \tilde{\mathbf{m}}^i) \right\| \leq \frac{2Lc_1c_u\eta\sqrt{d}}{\beta}, \quad (52)$$

1034 and

$$1035 \quad \mathbb{E} \left\| \tilde{\boldsymbol{\theta}}^k - \boldsymbol{\theta}^k \right\|^2 = \mathbb{E} \left\| \sum_{i=0}^k \boldsymbol{\eta}^i \circ (\mathbf{m}^i - \tilde{\mathbf{m}}^i) \right\|^2 \leq \frac{4c_1^2c_u^2\eta^2d}{\beta^2}. \quad (53)$$

1036 Based on the L -smooth assumption of the objective f , we have

$$\begin{aligned} 1037 \quad \mathbb{E}f(\boldsymbol{\theta}^{k+1}) &\leq \mathbb{E}f(\boldsymbol{\theta}^k) + \mathbb{E} \langle \nabla f(\boldsymbol{\theta}^k), \boldsymbol{\theta}^{k+1} - \boldsymbol{\theta}^k \rangle + \frac{L}{2} \mathbb{E} \|\boldsymbol{\theta}^{k+1} - \boldsymbol{\theta}^k\|^2 \\ 1038 \quad &= \mathbb{E}f(\boldsymbol{\theta}^k) - \mathbb{E} \langle \nabla f(\boldsymbol{\theta}^k), \boldsymbol{\eta}^k \circ \mathbf{m}^k \rangle + \frac{L}{2} \mathbb{E} \|\boldsymbol{\theta}^{k+1} - \boldsymbol{\theta}^k\|^2 \\ 1039 \quad &= \mathbb{E}f(\boldsymbol{\theta}^k) - \mathbb{E} \langle \nabla f(\tilde{\boldsymbol{\theta}}^k), \boldsymbol{\eta}^k \circ \mathbf{m}^k \rangle + \frac{L}{2} \mathbb{E} \|\boldsymbol{\theta}^{k+1} - \boldsymbol{\theta}^k\|^2 \\ 1040 \quad &\quad + \mathbb{E} \langle \nabla f(\tilde{\boldsymbol{\theta}}^k) - \nabla f(\boldsymbol{\theta}^k), \boldsymbol{\eta}^k \circ \mathbf{m}^k \rangle \\ 1041 \quad &\leq \mathbb{E}f(\boldsymbol{\theta}^k) - \mathbb{E} \langle \nabla f(\tilde{\boldsymbol{\theta}}^k), \boldsymbol{\eta}^k \circ \mathbf{m}^k \rangle + \frac{L}{2} \mathbb{E} \|\boldsymbol{\theta}^{k+1} - \boldsymbol{\theta}^k\|^2 + \frac{2Lc_1c_u c_\infty \eta^2 d}{\beta} \\ 1042 \quad &= \mathbb{E}f(\boldsymbol{\theta}^k) + \frac{1}{2} \mathbb{E} \left\| \sqrt{\boldsymbol{\eta}^k} \circ (\nabla f(\tilde{\boldsymbol{\theta}}^k) - \mathbf{m}^k) \right\|^2 - \frac{1}{2} \mathbb{E} \left\| \sqrt{\boldsymbol{\eta}^k} \circ \nabla f(\tilde{\boldsymbol{\theta}}^k) \right\|^2 \\ 1043 \quad &\quad - \frac{1}{2} \mathbb{E} \left\| \sqrt{\boldsymbol{\eta}^k} \circ \mathbf{m}^k \right\|^2 + \frac{L}{2} \mathbb{E} \|\boldsymbol{\eta}^k \circ \mathbf{m}^k\|^2 + \frac{2Lc_1c_u c_\infty \eta^2 d}{\beta} \\ 1044 \quad &\leq \mathbb{E}f(\boldsymbol{\theta}^k) + \frac{c_u\eta}{2} \mathbb{E} \left\| \nabla f(\tilde{\boldsymbol{\theta}}^k) - \mathbf{m}^k \right\|^2 - \frac{c_l\eta}{2} \mathbb{E} \left\| \nabla f(\tilde{\boldsymbol{\theta}}^k) \right\|^2 \\ 1045 \quad &\quad + \left(\frac{Lc_u^2\eta^2}{2} - \frac{c_l\eta}{2} \right) \mathbb{E} \|\mathbf{m}^k\|^2 + \frac{2Lc_1c_u c_\infty \eta^2 d}{\beta} \\ 1046 \quad &\leq \mathbb{E}f(\boldsymbol{\theta}^k) + \frac{c_u\eta}{2} \mathbb{E} \left\| \nabla f(\tilde{\boldsymbol{\theta}}^k) - \mathbf{m}^k \right\|^2 - \frac{c_l\eta}{2} \mathbb{E} \left\| \nabla f(\tilde{\boldsymbol{\theta}}^k) \right\|^2 \\ 1047 \quad &\quad - \frac{c_l\eta}{4} \mathbb{E} \|\mathbf{m}^k\|^2 + \frac{2Lc_1c_u c_\infty \eta^2 d}{\beta}. \end{aligned} \quad (54)$$

1048 For the first inequality we use (52). For the second inequality we use the upper and lower
 1049 bound of $\boldsymbol{\eta}$. For the third inequality we set $\eta \leq \frac{c_l}{2Lc_u^2}$. Then based on Lemma C.4 we have
 1050

$$1051 \quad \mathbb{E} \left\| \mathbf{m}^k - \nabla f(\tilde{\boldsymbol{\theta}}^k) \right\|^2 \leq (1 - \beta_1) \mathbb{E} \left\| \mathbf{m}^{k-1} - \nabla f(\tilde{\boldsymbol{\theta}}^{k-1}) \right\|^2 + \frac{(1 - \beta_1)^2 L^2}{\beta_1} \mathbb{E} \left\| \tilde{\boldsymbol{\theta}}^{k-1} - \tilde{\boldsymbol{\theta}}^k \right\|^2 + \frac{\beta_1^2 \sigma^2}{N}. \quad (55)$$

1052 For the second factor we have

$$1053 \quad \mathbb{E} \left\| \tilde{\boldsymbol{\theta}}^{k-1} - \tilde{\boldsymbol{\theta}}^k \right\|^2 \leq 3 \left(\mathbb{E} \left\| \boldsymbol{\theta}^{k-1} - \boldsymbol{\theta}^k \right\|^2 + \mathbb{E} \left\| \tilde{\boldsymbol{\theta}}^k - \boldsymbol{\theta}^k \right\|^2 + \mathbb{E} \left\| \tilde{\boldsymbol{\theta}}^{k-1} - \boldsymbol{\theta}^{k-1} \right\|^2 \right). \quad (56)$$

1080 Thus, we have
1081

$$\begin{aligned} \mathbb{E} \left\| \mathbf{m}^k - \nabla f(\tilde{\boldsymbol{\theta}}^k) \right\|^2 &\leq (1 - \beta_1) \mathbb{E} \left\| \mathbf{m}^{k-1} - \nabla f(\tilde{\boldsymbol{\theta}}^{k-1}) \right\|^2 + \frac{3c_u^2\eta^2(1 - \beta_1)^2L^2}{\beta_1} \mathbb{E} \|\mathbf{m}^{k-1}\|^2 \\ &\quad + \frac{\beta_1^2\sigma^2}{N} + \frac{24L^2c_1^2c_u^2\eta^2d}{\beta^2}. \end{aligned} \quad (57)$$

1086 By adding equation (54) at $\boldsymbol{\theta}^{k+1}$ and $a \times$ equation (57) at $\boldsymbol{\theta}^{k+1}$, we have
1087

$$\begin{aligned} \mathbb{E} f(\boldsymbol{\theta}^{k+1}) + a \mathbb{E} \left\| \mathbf{m}^{k+1} - \nabla f(\tilde{\boldsymbol{\theta}}^{k+1}) \right\|^2 &\leq \mathbb{E} f(\boldsymbol{\theta}^k) + \left(\frac{c_u\eta}{2} + a(1 - \beta_1) \right) \mathbb{E} \left\| \nabla f(\tilde{\boldsymbol{\theta}}^k) - \mathbf{m}^k \right\|^2 \\ &\quad - \frac{c_l\eta}{2} \mathbb{E} \left\| \nabla f(\tilde{\boldsymbol{\theta}}^k) \right\|^2 - \left(\frac{c_l\eta}{4} - \frac{3ac_u^2\eta^2(1 - \beta_1)^2L^2}{\beta_1} \right) \mathbb{E} \|\mathbf{m}^k\|^2 \\ &\quad + \frac{a\beta_1^2\sigma^2}{N} + \frac{2Lc_1c_u c_\infty \eta^2 d}{\beta} + \frac{24aL^2c_1^2c_u^2\eta^2d}{\beta^2}. \end{aligned} \quad (58)$$

1096 Letting $a = \frac{\eta c_u}{\beta_1}$ and $G(\boldsymbol{\theta}^k) = \mathbb{E} f(\boldsymbol{\theta}^k) + \frac{\eta c_u}{\beta_1} \mathbb{E} \left\| \mathbf{m}^{k+1} - \nabla f(\tilde{\boldsymbol{\theta}}^{k+1}) \right\|^2$, we have
1097

$$\begin{aligned} G(\boldsymbol{\theta}^{k+1}) &\leq G(\boldsymbol{\theta}^k) - \frac{c_l\eta}{2} \mathbb{E} \left\| \nabla f(\tilde{\boldsymbol{\theta}}^k) \right\|^2 - \left(\frac{c_l\eta}{4} - \frac{3c_u^3\eta^3(1 - \beta_1)^2L^2}{\beta_1^2} \right) \mathbb{E} \|\mathbf{m}^k\|^2 \\ &\quad + \frac{c_u\eta\beta_1\sigma^2}{N} + \frac{2Lc_1c_u c_\infty \eta^2 d}{\beta} + \frac{24L^2c_1^2c_u^3\eta^3d}{\beta_1\beta^2} \\ &\leq G(\boldsymbol{\theta}^k) - \frac{c_l\eta}{2} \mathbb{E} \left\| \nabla f(\tilde{\boldsymbol{\theta}}^k) \right\|^2 - \frac{c_l\eta}{8} \mathbb{E} \|\mathbf{m}^k\|^2 \\ &\quad + \frac{c_u\eta\beta_1\sigma^2}{N} + \frac{2Lc_1c_u c_\infty \eta^2 d}{\beta} + \frac{24L^2c_1^2c_u^3\eta^3d}{\beta_1\beta^2}, \end{aligned} \quad (59)$$

1108 where we set $\eta \leq \frac{\beta_1 c_l^{0.5}}{5c_u^{1.5}(1 - \beta_1)L}$. Then we sum the inequality above from $k = 0$ to $K - 1$ and
1109 obtain
1110

$$\begin{aligned} \frac{1}{K} \sum_{k=0}^{K-1} \mathbb{E} \left[\left\| \nabla f(\tilde{\boldsymbol{\theta}}^k) \right\|^2 + \frac{1}{4} \|\mathbf{m}^k\|^2 \right] &\leq \frac{2(G(\boldsymbol{\theta}^0) - G(\boldsymbol{\theta}^K))}{\eta c_l K} + \frac{2c_u\beta_1\sigma^2}{c_l N} + \frac{4Lc_1c_u c_\infty \eta d}{c_l \beta} \\ &\quad + \frac{48L^2c_1^2c_u^3\eta^2d}{c_l \beta_1 \beta^2}. \end{aligned} \quad (60)$$

1116 Considering that
1117

$$\begin{aligned} G(\boldsymbol{\theta}^0) - G(\boldsymbol{\theta}^K) &\leq \mathbb{E} f(\boldsymbol{\theta}^0) - \mathbb{E} f(\boldsymbol{\theta}^K) + \frac{\eta c_u}{\beta_1} \mathbb{E} \left\| \mathbf{m}^0 - \nabla f(\tilde{\boldsymbol{\theta}}^0) \right\|^2 \\ &\leq \mathbb{E} f(\boldsymbol{\theta}^0) - \mathbb{E} f(\boldsymbol{\theta}^*) + \frac{\eta c_u \sigma^2}{\beta_1 N}, \end{aligned} \quad (61)$$

1122 and letting $\mathbb{E} f(\boldsymbol{\theta}^0) - \mathbb{E} f(\boldsymbol{\theta}^*) = \Delta$, we have
1123

$$\begin{aligned} \frac{1}{K} \sum_{k=0}^{K-1} \mathbb{E} \left[\left\| \nabla f(\tilde{\boldsymbol{\theta}}^k) \right\|^2 + \frac{1}{4} \|\mathbf{m}^k\|^2 \right] &\leq \frac{2\Delta}{\eta c_l K} + \frac{2c_u\sigma^2}{c_l K \beta_1 N} + \frac{2c_u\beta_1\sigma^2}{c_l N} + \frac{4Lc_1c_u c_\infty \eta d}{c_l \beta} \\ &\quad + \frac{48L^2c_1^2c_u^3\eta^2d}{c_l \beta_1 \beta^2}. \end{aligned} \quad (62)$$

1129 Finally setting $K = \Omega(d\epsilon^{-4})$, $\eta = \mathcal{O}(d^{-1}\epsilon^2)$ and $\beta_1 = \mathcal{O}(d^{-1}\epsilon^2)$, we have
1130

$$\frac{1}{K} \sum_{k=0}^{K-1} \mathbb{E} \left[\left\| \nabla f(\tilde{\boldsymbol{\theta}}^k) \right\|^2 + \frac{1}{4} \|\mathbf{m}^k\|^2 \right] \leq \mathcal{O}(\epsilon^2). \quad (63)$$

1133 We end the proof of Theorem 5.7. \square

1134 D LOW-RANK PROPERTY OF GRADIENT IN TRAINING DYNAMIC
 1135

1136 In this section, we give an simple theoretical analysis to demonstrate that the gradient of
 1137 project-up layers of MLP in Transformer-based models becomes low-rank with training time.
 1138 Our analysis is based on recent study on the framework of Transformer dynamic, JoMA [50],
 1139 and fix an error in related study [64].

1140 We follow the definitions and assumptions of Transformer in JoMA [50], and compute the
 1141 dynamic of project-up layer in Transformer MLP as below.

1142 **Lemma D.1.** Suppose the embedding matrix $\mathbf{U} \in \mathbb{R}^{m \times M}$ is fixed, where M represents the
 1143 vocabulary size. The active function is linear and the back propagation gradient is stationary
 1144 [50]. The weight matrix is $\mathbf{W} \in \mathbb{R}^{m \times n}$. Let $\Delta = [\Delta_1, \dots, \Delta_n]$, where $\Delta_j = \mathbb{E}_q[g_j \mathbf{x}] \in \mathbb{R}^M$.
 1145 g_j is the back propagated gradient of hidden node j in MLP, \mathbb{E}_q represents the conditional
 1146 expectation given the query q , and \mathbf{x} represents the token distribution in the previous layer,
 1147 for example, the activation output of the previous layer. Following the same definitions and
 1148 assumptions in JoMA [50], the project-up matrix $\mathbf{V} = \mathbf{U}^\top \mathbf{W} \in \mathbb{R}^{M \times n}$ satisfies

$$1149 \quad \dot{\mathbf{V}} = \frac{1}{A} \exp\left(\frac{\mathbf{V} \circ \mathbf{V}}{2}\right) \circ \Delta, \quad (64)$$

1150 where A is the normalization of softmax.
 1151

1152 *Proof.* Let $\mathbf{V} = [\mathbf{v}_1, \dots, \mathbf{v}_n]$ and $\mathbf{W} = [\mathbf{w}_1, \dots, \mathbf{w}_j]$. Following the Theorem 2 in study of
 1153 JoMA framework [50], for each hidden node j , $\mathbf{v}_j = \mathbf{U}^\top \mathbf{w}_j$ satisfies

$$1154 \quad \dot{\mathbf{v}}_j = \frac{1}{A} \Delta_j \circ \exp(\mathbf{v}_j^2/2), \quad (65)$$

1155 where $\mathbf{v}_j^2 = \mathbf{v}_j \circ \mathbf{v}_j$ is the element-wise product of vector. Then we notice that Lemma D.1
 1156 is the matrix form of equation (65). \square
 1157

1158 With Lemma D.1, we analyse the training dynamic of \mathbf{V} . Row-wisely write \mathbf{V} as $\mathbf{V} =$
 1159 $[\mathbf{u}_1^\top, \dots, \mathbf{u}_M^\top]^\top$ and Δ as $\Delta = [\delta_1^\top, \dots, \delta_M^\top]^\top$. Based on Lemma D.1, for $j \in [M]$, we have

$$1160 \quad \dot{\mathbf{u}}_j = \frac{1}{A} \exp(\mathbf{u}_j^2/2) \circ \delta_j = \frac{1}{A} \text{diag}(\exp(\mathbf{u}_j^2/2)) \delta_j \quad (66)$$

1161 Based on the assumption that the back propagation gradient is stationary and \mathbf{x} is the
 1162 output of previous layer, which means it is given. Thus the Δ_j is constant, and the direction
 1163 of \mathbf{u}_j is controlled by a diagonal matrix. Let $\dot{\mathbf{u}}_j = \mathbf{D}_j(t) \delta_j$, where $\mathbf{D}_j(t)$ is a diagonal matrix
 1164 with initialization $\mathbf{D}_j(0) = \mathbf{0}$. Then we have

$$1165 \quad \dot{\mathbf{D}}_j(t) = \frac{1}{A} \text{diag}\left(\exp\left(\frac{\mathbf{D}_j^2(t) \delta_j^2}{2}\right)\right). \quad (67)$$

1166 Let $a_j^2 = \max_{i \in [n]} \delta_{ji}^2$ and $b_j^2 = \min_{i \in [n]} \delta_{ji}^2$. Then we have

$$1167 \quad \frac{1}{A} \text{diag}\left(\exp\left(\frac{\mathbf{D}_j^2(t) b_j^2}{2}\right)\right) \preceq \dot{\mathbf{D}}_j(t) \preceq \frac{1}{A} \text{diag}\left(\exp\left(\frac{\mathbf{D}_j^2(t) a_j^2}{2}\right)\right). \quad (68)$$

1168 Element-wisely analyze the diagnoal matrix $\mathbf{D}_j(t) = \text{diag}(d_{j1}(t), \dots, d_{jn}(t))$. For $i \in [n]$,
 1169 we have

$$1170 \quad \frac{1}{A} \exp\left(\frac{d_{ji}^2(t) b_j^2}{2}\right) \leq d_{ji} \leq \frac{1}{A} \exp\left(\frac{d_{ji}^2(t) a_j^2}{2}\right). \quad (69)$$

1171 For dynamic like $\dot{x} = C e^{\beta^2 x^2}$, we have

$$1172 \quad x(t) = \frac{1}{\beta} \text{erf}^{-1}\left(\frac{2\beta C}{\sqrt{\pi}} t\right), \quad (70)$$

1188
1189 Table 4: Comparison of SEPARATE with previous common gradient compression algorithms
1190 in standard application metrics, including gradient complexity , real communication time,
1191 memory cost, ring-based communication support, and sharding support. Here, Ψ represents
1192 the scale of model parameters, N represents the number of nodes in distributed cluster,
1193 B is the communication bandwidth (bytes/s), r is the dimension of low-rank subspace of
1194 gradient to PowerSGD, and m is the random Gaussian samples in SEPARATE in Algorithm
1195 1. Here we only consider the order of ϵ in gradient complexity, ignoring others especially the
1196 dimension of parameters d . We discuss the order of d in detail in Section 5. We consider the
1197 mixed-precision setting for memory overhead.

| Methods | Gradient Complexity | Communication Cost | Memory Cost | Ring-based Comm. | Gradient Sharding |
|-----------------|------------------------------|---------------------------|--------------------------|------------------|-------------------|
| SGD | $\mathcal{O}(\epsilon^{-4})$ | $4\Psi(N-1)/(BN)$ | $2\Psi + 6\Psi/N$ | ✓ | ✓ |
| Adam [27] | $\mathcal{O}(\epsilon^{-4})$ | $4\Psi(N-1)/(BN)$ | $2\Psi + 14\Psi/N$ | ✓ | ✓ |
| 1-bit Adam [49] | $\mathcal{O}(\epsilon^{-4})$ | $0.625\Psi N/B$ | 18Ψ | ✗ | ✗ |
| 1-bit LAMB [29] | $\mathcal{O}(\epsilon^{-4})$ | $0.625\Psi N/B$ | 22Ψ | ✗ | ✗ |
| PowerSGD [55] | ✗ | $4r\sqrt{\Psi}(N-1)/(BN)$ | $14\Psi + 2r\sqrt{\Psi}$ | ✓ | ✓ |
| SEPARATE-SGD | $\mathcal{O}(\epsilon^{-4})$ | $4m(N-1)/(BN)$ | $4\Psi + 6\Psi/N$ | ✓ | ✓ |
| SEPARATE-Adam | $\mathcal{O}(\epsilon^{-4})$ | $4m(N-1)/(BN)$ | $4\Psi + 14\Psi/N$ | ✓ | ✓ |

1209
1210 Table 5: Compare SEPARATE with LoRA. Suppose that the weight matrix $\mathbf{W} \in \mathbb{R}^{m \times n}$, the
1211 low-rank reparameterized size of LoRA is r , and the compression ratio of SEPARATE is k .

| | SEPARATE | LoRA |
|------------|----------|----------------|
| Weight | mn | $mn + nr + mr$ |
| Grad Comm. | mn/k | $nr + mr$ |
| Pre-train | ✓ | ✗ |
| Fine-tune | ✓ | ✓ |

1217 where $\text{erf}(x)$ is Gaussian error function. Then we have

$$\frac{\sqrt{2}}{b_j} \text{erf}^{-1} \left(\sqrt{\frac{2}{\pi A}} b_j t \right) \leq d_{ji}(t) \leq \frac{\sqrt{2}}{a_j} \text{erf}^{-1} \left(\sqrt{\frac{2}{\pi A}} a_j t \right). \quad (71)$$

1222 Since the bound is independent of i , for each j we have

$$\frac{\sqrt{2}}{b_j} \text{erf}^{-1} \left(\sqrt{\frac{2}{\pi A}} b_j t \right) \mathbf{I} \preceq \mathbf{D}_j(t) \preceq \frac{\sqrt{2}}{a_j} \text{erf}^{-1} \left(\sqrt{\frac{2}{\pi A}} a_j t \right) \mathbf{I}. \quad (72)$$

1227 It demonstrates that for each line of \mathbf{V} , the direction of \mathbf{u}_j is near to the direction of δ_j with
1228 error dependent to a_j and b_j . Next we show that the change of direction from one line to
1229 another is very different resulting in low-rank property of \mathbf{V} . Let

$$h(t, a) = \frac{\sqrt{2}}{a} \text{erf}^{-1} \left(\sqrt{\frac{2}{\pi A}} a t \right). \quad (73)$$

1234 Then we have $h(t, b_j) \mathbf{I} \preceq \mathbf{D}_j(t) \preceq h(t, a_j) \mathbf{I}$. Considering $\lim_{t \rightarrow \sqrt{\pi A}/\sqrt{2}a} h(t, a) \rightarrow +\infty$, let
1235 $j^* = \arg \max_j b_j$ be the row with the largest entry of b_j . Then if $b_{j^*} \geq a_j$ for all $j \neq j^*$,
1236 when $t \rightarrow t^* = \sqrt{\pi A}/\sqrt{2}b_{j^*}$, we have $\mathbf{D}_{j^*}(t) \succeq h(t, b_{j^*}) \mathbf{I} \rightarrow +\infty$ but $\mathbf{D}_j(t) \preceq h(t, a_j) \mathbf{I}$ is still
1237 finite because $t' = \sqrt{\pi A}/\sqrt{2}a_j \geq t^*$.

1239 Such analysis demonstrates that the magnitude of each row of \mathbf{V} changes drastically. The
1240 dominant direction of \mathbf{V} will become extremely large when others are still in a small range
1241 over time. \mathbf{V} will become near rank-1 over time and $\dot{\mathbf{V}}$ has lower rank because $\dot{\mathbf{D}}$ have \mathbf{D} on
exponents. Such analysis is consistent with what we observed in Figure 1 in Section 3.

1242

1243 Table 6: Performance comparison with LoRA. We fine-tune LLAMA2-7B on the alpaca-
 1244 gpt4 dataset and evaluate the performance on downstream tasks, including commonsense
 1245 reasoning, world knowledge, math, and code.

1246

| Method | TriQA | GSM8K | MBPP | NQ | WinoG | Arc-e | Arc-c | PIQA | Avg. |
|-----------|--------------|--------------|--------------|-------------|--------------|--------------|--------------|--------------|--------------|
| Adam | 49.39 | 15.69 | 19.40 | 3.07 | 46.09 | 72.31 | 53.90 | 57.07 | 39.62 |
| Adam-LoRA | 62.08 | 16.53 | 16.80 | 5.15 | 49.57 | 49.21 | 37.97 | 52.88 | 36.27 |
| SEPARATE | 57.18 | 20.17 | 21.40 | 4.18 | 49.25 | 72.66 | 49.83 | 52.99 | 40.96 |

1250

1251

E EXPEIMENT DETAILS

1252

E.1 MODEL CONFIGURATIONS

1253

1254

We pre-train the GPT-2-345M [40] model on OpenWebtext dataset [17] of 10B tokens from scratch. We show the results in Figure 2. Second, we compare the SEPARATE with several representative baselines to fine-tune the LLAMA2-7B model and evaluate on downstream tasks. The baselines include typical low-rank optimizers with error feedback technique like PowerSGD [55], representative low-bit optimizers like 1-bit Adam [49], and recent quantization efficient training strategy ZeRO++ [56]. For fairness, we use SEPARATE-based Adam for comparison. In this section, we propose the experiment details including model and hyper-parameters settings. Without special emphasis all experiments are under bfloat16 precision.

1255

1256

GPT-2. We conducted the training of GPT-2-345M model [40] from scratch on the OpenWebtext [17] dataset on $8 \times$ NVIDIA 3090 24G GPUs cluster. We ran a total of 50000 iterations and processed a total of 10B tokens. The experiment was configured with PyTorch DDP training framework without model and pipeline parallelism to simplify the experimental setting and fit existing devices. Our global batch size was 8×512 . We set the learning rate at 6.0e-4 with the cosine decay down to the minimum 6.0e-5 after 2000 iterations of warm-up. We also used the gradient accumulation and set the gradient accumulation step at 4. We used the global gradient norm clipping of 1 and set the Adam with $\beta_1 = 0.9$ and $\beta_2 = 0.95$.

1257

1258

LLAMA2-7B. We conducted the fine-tuning of LLAMA2-7B [51] model on alpaca-gpt4 dataset [39] within the PyTorch FSDP [65] framework. We followed protocols from LLAMA-Accessory [63] and fine-tuned LLAMA2-7B for three epochs on $8 \times$ NVIDIA A6000 48G GPUs cluster. To fit the devices we set the data parallelism at 4 and model parallelism at 2 without pipeline parallelism. We set the global batch size at 32, the learning rate of 2e-5, gradient clipping of 2 and gradient accumulation step at 8.

1259

1260

Following the previous work [63], we conducted evaluation on chosen benchmarks on the popular OpenCompass [12] platform. We chose the benchmarks including commonsense reasoning, world knowledge, math and code as follows:

1261

1262

1263

- Commonsense Reasoning: Hellaswag [62], Winogrande [45], ARC-Easy [10], ARC-Challenge [10] and PIQA [7].
- World Knowledge: NaturalQuestions [28] and TriviaQA [26].
- Math: GSM8K [11].
- Code: MBPP [4].

1264

1265

E.3 APPLICATION TO TRAINING PROCESS AS A PLUG-IN

1266

1267

1268

1269

1270

1271

1272

1273

1274

1275

1276

1277

SEPARATE can be easily applied to real large-scale model training tasks. SEPARATE only needs small amount of extra computation costs, which can be formulated as tensor multiplication form that is well supported by modern computational device architectures like CUDA [35]. By using **hook** mechanism in PyTorch, we can compress the latter layer’s gradient and do communication while the optimizer computes the former layer’s gradient

1296 **Algorithm 3** G-SEPARATE: General Version of Simple Low-rank Projection
1297 **Require:** Initialization model parameters with L layers, N nodes, layer-wise communication
1298 ratio $\{m_l\}_{l=1}^L$, layer-wise $\{\beta_l\}_{l=1}^L$, $\beta_l = 0.95, \forall l \in [L]$, error reset frequency T_e , adaptive
1299 update frequency T_a , a common Gaussian random number generator, initialize $\mathbf{e}^0 \in \mathcal{B}(\mathbf{0}, c_1)$
1300 **while** $k \leq K$ **do**
1301 STEP 1. In each node n compute stochastic gradient $\mathbf{g}_{n,l}^k$ and $\mathbf{h}_{n,l}^k = \mathbf{g}_{n,l}^k + \mathbf{e}_{n,l}^k$;
1302 STEP 2. Generate fresh i.i.d. common random Gaussian vectors $\xi_1, \dots, \xi_{m_l^k} \sim N(0, \mathbf{I}_d)$
1303 and compute $[p_{1,n,l}, \dots, p_{m_l^k,n,l}]$ with $p_{i,n,l} = \langle \mathbf{h}_{n,l}^k, \xi_i \rangle$ as the low-dimension
1304 projection of $\mathbf{h}_{n,l}^k$;
1305 STEP 3. Do all-reduce and obtain global projected gradient $[\tilde{p}_{1,l}, \dots, \tilde{p}_{m_l^k,l}]$;
1306 STEP 4. Compute $\tilde{\mathbf{h}}_{n,l}^k = \frac{1}{m_l^k} \sum_{i=1}^{m_l^k} \tilde{p}_{i,l} \cdot \xi_i$ and use $\tilde{\mathbf{h}}_{n,l}^k$ for model weight update
1307 in node n ;
1308 STEP 5. Update error
1309 $\mathbf{e}_{n,l}^{k+1} = (1 - \beta_l^k) \mathbf{e}_{n,l}^k + \beta_l^k (\mathbf{h}_{n,l}^k - \tilde{\mathbf{h}}_{n,l}^k)$ if $k \% T_e \neq 0$,
1310 $\mathbf{e}_{n,l}^{k+1} = 0$ if $k \% T_e = 0$ (error reset);
1311 STEP 6. Layer-wisely update compression ratio and β_l
1312 $m_l^{k+1} = \text{int} \left(1 + m_l^k \cdot \left(1 + \frac{\langle \tilde{\mathbf{h}}_{n,l}^k, \mathbf{g}_{n,l}^k \rangle}{\|\tilde{\mathbf{h}}_{n,l}^k\| \cdot \|\mathbf{g}_{n,l}^k\|} \right) \right)$,
1313 $\beta_l^{k+1} = \max \left\{ \min \left\{ \beta_l^k \cdot \left(1 + \frac{\langle \tilde{\mathbf{h}}_{n,l}^k, \mathbf{g}_{n,l}^k \rangle}{\|\tilde{\mathbf{h}}_{n,l}^k\| \cdot \|\mathbf{g}_{n,l}^k\|} \right), 0.99 \right\}, 0.90 \right\}$ if $k \% T_a = 0$,
1314 $m_l^{k+1} = m_l^k$,
1315 $\beta_l^{k+1} = \beta_l^k$, if $k \% T_a \neq 0$;
1316 **end while**
1317
1318
1319
1320
1321
1322
1323
1324
1325
1326
1327
1328
1329
1330
1331
1332
1333
1334
1335
1336
1337
1338
1339
1340
1341
1342
1343
1344
1345
1346
1347
1348
1349

in backpropagation process. Thus we properly arrange the overlapped computation and communication order, the time cost of compression can be hidden in the backpropagation computation, and SEPARATE can realize faster training time. Moreover, SEPARATE can be applied to ring-based or tree-based communication. Different from quantization methods, SEPARATE is not troubled by numerical anomalies like overflow or underflow, so it well supports reduce-scatter operation. SEPARATE also supports sharding strategy which is commonly used for training large language models [41]. Even though the gradient is separated into different nodes, the linearity of random projection ensures the correctness of SEPARATE’s results. We propose an example that how to use SEPARATE as a plug-in by hook mechanism in Algorithm 2.

Besides, SEPARATE brings extra memory costs for training because of the store of error and random variables. Setting up a random variable buffer, we can reduce the memory costs by reusing this part of memory to store the stream of random variables. In summary, from the results in Table 4, it is evident that SEPARATE demonstrates superior properties compared to other methods.

E.4 ADDITIONAL EXPERIMENTS

Parameter-efficient fine-tuning (PEFT) techniques accelerate the application of pre-trained language models to different downstream tasks without the need to fine-tune all of the model’s parameters [14]. Among them, the popular Low-Rank Adaptation (LoRA [22]) reparameterizes the weight matrix to low-rank approximations and fine-tuning the reparameterized ones. We compare SEPARATE with popular LoRA on scopes of application and performance on downstream tasks in Table 5 and Table 6. The results demonstrate that SEPARATE has better versatility and effect than LoRA.

E.5 GENERAL VERSION OF SIMPLE LOW-RANK PROJECTION

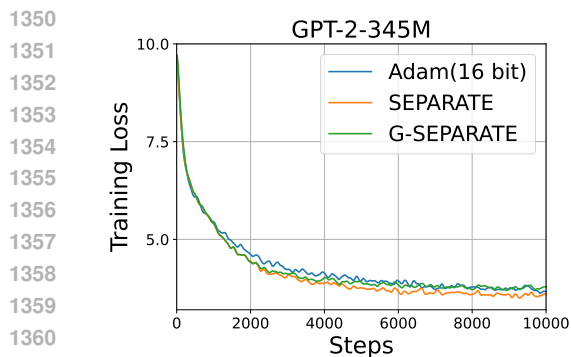


Figure 4: Loss curve of vanilla Adam, SEPARATE with compression ratio 8, and G-SEPARATE on GPT-2-345M trained with 10B tokens OpenWebtext dataset.

In this section, we study how to adaptively select the compression ratio and β for moving average error feedback. We expect to dynamically adjust these hyperparameters by combining the characteristics of the parameters at each layer of the model and the training dynamic. Our research focuses on two aspects. First, the adaptive strategy needs to remain simple and efficient to ensure the overall training wall-clock time is reduced. Thus, we still do not consider the strategies that require periodic heavy computations, such as periodic SVD. Second, considering the robustness of our method shown in Appendix A, we think the dynamic adjustment of hyperparameters should not be too sharp to avoid instability in training. Under this consideration, we get the general version of SEPARATE in Algorithm 3.

We layer-wisely compute the cosine similarity of the gradient estimate and the gradient itself frequently to evaluate the estimate accuracy, and update the compression ratio and β in moving average error feedback dynamically. As shown in Algorithm 3 STEP 6, if the estimate is accurate, we try to use a more aggressive compression ratio and a larger β in the next stage, and vice versa. All steps in Algorithm 3 are layer-wise, and we use the subscript l to represent the operation on the l -th layer. The initialization of m_l can be arbitrary such as 16, 32 or 64. The adaptive mechanism can adjust it to the proper region of the corresponding layer through several dynamic update processes.

We pre-train GPT-2-345M on 10B tokens OpenWebtext dataset from scratch to verify the effectiveness of G-SEPARATE. We follow the same hyperparameter setting of our pre-training experiment in Appendix E.1. For G-SEPARATE, we set the adaptive update frequency $T_a = 2000$ to ensure the stability of training. The results shown in Figure 4 indicate that the adaptive extension more slightly fits the baseline, but shares the similar performance of the original algorithm in total.